8-1-1997

Materials for attenuated phase mask application at 193 nm

Shahid Butt

Materials for Attenuated Phase Shift Mask Application at 193 nm

By Shahid Butt
Rochester Institute of Technology
Materials Science and Engineering

Masters of Science thesis

August 1997

Materials For Attenuated Phase Mask application at 193 nm.

by

Shahid Butt

_____

Shahid Butt

Materials for Attenuated Phase Mask application at 193 nm

by

Shahid Butt

A thesis submitted in partial fulfillment of the requirements for the degree of

Master of Science

in Materials Science and Engineering at the Rochester Institute of Technology.

Approved by.

Dr. Bruce Smith, Advisor
Department of Microelectronic Engineering & Materials Science and Engineering.

Dr. Santosh Kurinec
Department of Microelectronic Engineering & Materials Science and Engineering.

Dr. Richard Lane
Department of Microelectronic Engineering & Materials Science and Engineering

Dr. Vern Lindberg
Department of Physics & Materials Science and Engineering

Table of Contents

List of Figures

List of Tables

Abstract

The electronic revolution is driven by the circuits and devices fabricated on silicon. Since the invention of the integrated circuit some thirty years ago the circuit complexity has increased manifold. A large portion of this increase can be attributed to the ability to print smaller features. The process of printing these small features is termed lithography. The ability to develop new lithographic techniques will determine to a large extent whether the semiconductor industry can maintain its rapid growth rate. Currently lithographic techniques that utilize 193 nm radiation are being dev loped to replace the 248 nm based lithographic processes. The trend towards smaller features has meant development of optics and materials that can be used at shorter wavelengths. It has also meant the implementation of optical enhancement techniques, to extend the useful lifetime of the available technology.

Phase shift technology is currently being developed to extend the useful lifetime of 193 nm based systems. Of the various types of phase shift masks, the attenuated phase shift type seems attractive because they are relatively easy to manufacture. However, at shorter wavelengths the number of materials that can be used as single layer shifters is few. The situation is further aggravated by the additional requirements placed on mask material, such as minimal transmission at alignment wavelength, low resistivity and the ability to be dry etched.

The fore-mentioned requirements preclude the use of stoichiometric elements and compounds as materials suitable for a single layer attenuated phase shift mask. However, it may be possible to combine a variety of materials to obtain the desired optical and physical properties. By carefully choosing the absorbing and the non-absorbing components of the material mix, the optical and the physical properties can be engineered to meet the specifications. In case of thin films, the material properties can be varied by adjusting the deposition conditions. For this work reactive sputtering was used to deposit the films. By adjusting the partial pressure, power and time, and through the use of mosaic targets the material properties were investigated. Furthermore, films were also deposited in a layered structure that allowed for a new set of film properties.

Several materials were investigated for this work. By following a simple process of elimination the material was first evaluated for its optical properties followed by an evaluation of its physical properties. Films that were investigated were composed of molybdenum silicon oxide, under-stoichiometric aluminum nitride, under-stoichiometric silicon nitride and layered films of tantalum and silicon nitride. The primary selection factor for these films were there optical properties around 193 nm. Following this the films were evaluated for there properties in the visible regime. Finally the films were evaluated for there physical properties, such as stability and volatility of the etched compounds. Only under-stoichiometric aluminum nitride met all the requirements for attenuated phase shift mask material.

1.0 Introduction

Since the invention of the integrated circuit the number of components on a chip has doubled approximately every two years [1]. The increase in the number of components has been due to either an increase in area of the chip or due to the reduction in the size of the component. The increase in the number of components has led to better performing microchips. Figure 1 shows the size of the smallest feature on a chip, also termed as the critical dimension (CD), as a function of the year of production.

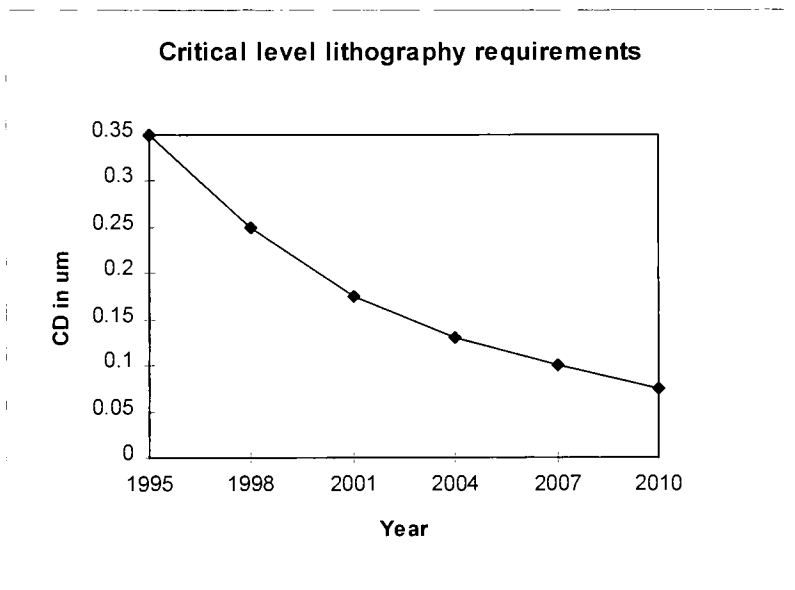

Figure 1: Critical dimension as a function of year.

The process of forming these small features is called lithography. It has been one of the major driving forces behind the rapid growth of the electronic industry. It is fair to say that the future of the semiconductor industry is dependent on its ability to print small patterns, and hence on lithography.

Most commonly the process of forming these small features utilizes some sort of an optical system that replicates the pattern present on a mask. A mask is a fused silica

blank with transparent and opaque regions. The opaque regions are generally formed by a thin chrome film. The mask is generally manufactured by using an electron beam writing tool, which focuses a beam of electrons onto an organic material called resist. The areas of the resist that has been exposed to the electrons become soluble and hence the resist can be removed selectively. The pattern is transferred by etching away the chrome and leaving transparent regions behind. A similar approach is used for transferring the pattern into the silicon, instead of using electrons to image the resist however photons are used. The areas of the resist that are exposed to the photons are representative of the pattern present on the mask. During the lithographic process the quality of the image or the size of the smallest feature that can be printed is a function of the optical imaging system, the photoresist and of the mask that is being used.

2.0 Theory

The resolution of a diffraction limited optical imaging system is given by the following relationship [2]

$$L = k_1\lambda/NA$$

where L is the minimum resolvable image, k_1 is a proportionality constant which depends on the coherence of the illumination, λ is wavelength of illumination and NA is a measure of the acceptance angle of the objective lens, a large acceptance angle implies that more of the diffracted light can be collected.

Another important issue is the depth of focus (DOF), which is the distance over which defocus is tolerable, the following equation relates DOF to λ and NA.

$$DOF = k_2\lambda/NA^2$$

where k_2 is another proportionality constant that is a function of the behavior of the resist and the image formed by the optics. Figure 2 and Figure 3 show how wavelength and NA affect depth of focus and CD.

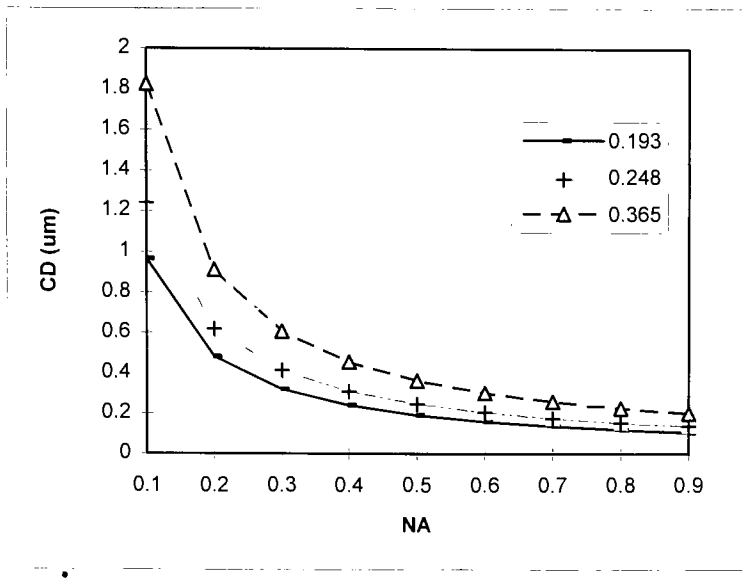

Figure 2: Effect of numerical aperture and wavelength on CD.

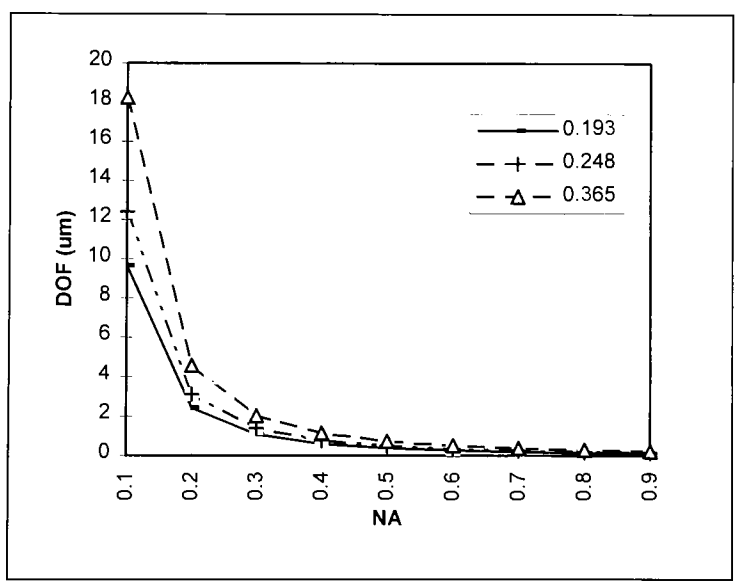

Figure 3: Effect of numerical aperture and wavelength on DOF.

It can be seen from Figure 2 and Figure 3 that for a given CD a larger depth of focus may be realized by using a shorter wavelength instead of a larger NA. This is because depth of focus is inversely proportional to the square of numerical aperture but proportional to the wavelength.

However, for economic reasons, it is desirable to stay with proven technology e.g. in the mid 80's, industry focused on the development of 248 nm lithography as a replacement of i-line (365 nm) based systems. It was believed that 248 nm would be the wavelength of choice for the 0.5 μm generation, however manufacturing lines are currently using i-line for the 0.35 μm generation [3]. Due to advancement in processing techniques and lens design it is now believed that 248 nm would be the technology of choice for the 0.18 μm generation and the 193 nm based systems would be used for the 0.13 μm generation. Hence, 248 nm and 193 nm exposure systems would be used in manufacturing when the critical dimensions become comparable with exposure wavelength. To extend the lifetime of these tools and to realize a bigger process window, optical enhancement techniques would be required. One such technique is through the use of Attenuated Phase Shift Masks (APSM), for realizing a larger depth of focus. Figure 4 illustrates how an APSM works as compared with a regular binary illumination mask.

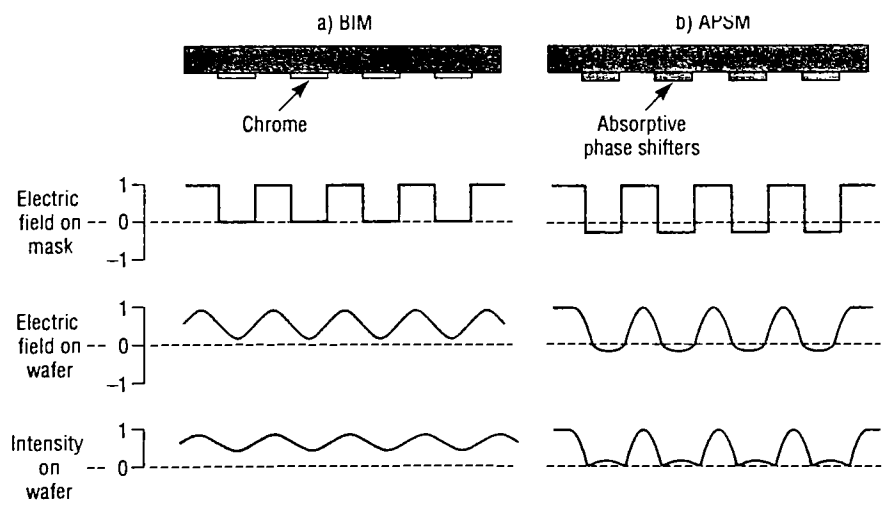

Figure 4: Comparison between a conventional mask and an attenuated PSM, from ref 4.

A conventional chrome on glass mask is similar to a diffraction grating, combining areas of 100% transmission with areas of zero transmission. The intent is to have maximum intensity in the clear regions and zero under the opaque regions.

However, due to diffraction, the intensity of the light does not go to zero under the opaque regions, making it harder to transfer the pattern. In an attenuated phase shift mask, the zero transmission areas are replaced by partially transmitting areas, which also changes the phase of the light by 180^0 relative to the clear regions. Due to the negative electric field under the partially transmitting regions the intensity must become zero at the boundary between clear and dark regions, hence the image contrast is increased. A common metric used for measuring the contrast is the image log slope, which is the slope of the aerial image formed at the interface of the clear and the dark regions. The improvement in the image log slope by using an APSM as compared to a conventional mask is illustrated in Figure 5.

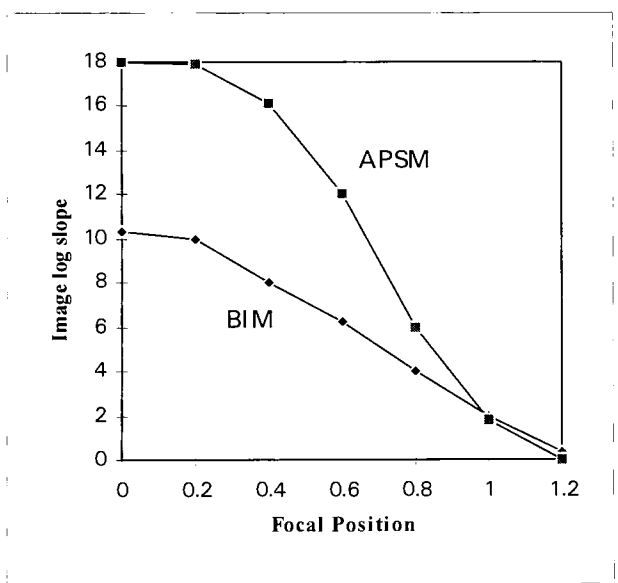

Figure 5: The improvement in image log slope gained by using an APSM over a conventional mask

2.1 Fundamental parameters of an APSM

From basic electromagnetic theory, the thickness required to obtain a 180^0 phase shift is given by the following relation, [5]:

$$d = \lambda/2(n-1)$$

where d is the thickness of the layer which shifts the phase, λ is the wavelength and n is the real part of the refractive index at that wavelength. The transmission obtained for a given thickness d is:

$$\alpha = 4\pi k/\lambda = -\ln (T)/d$$

$$\text{or} \qquad T=e^{-4\pi kd/\lambda}$$

where T is the transmission, k is the extinction coefficient of the material at that wavelength and d is the thickness. Another important parameter is the reflectivity of the mask. Any increase in reflectivity would lead to stray light in the optical system and hence degradation of the image. Single surface reflectance of any material is given by the following relation:

$$R = [(n-1)^2 + k^2]/ [(n+1)^2 + k^2]$$

where n and k are the refractive index and the extinction coefficient of the material at a given wavelength.

The effect of the film interface on the phase change cannot be ignored. Whenever light passes from one medium to another there is an associated phase change at the interface of the two; this phenomenon is described by the following relationship [6]:

$$\phi_{12} = \arg (2N_2/(N_1+N_2))$$

where $N_1 = n- ik$, which is the complex refractive index of the material through which the light is propagating and N_2 is the index of the material on which the light is incident. Figure 6 illustrates this effect, where phase change is represented in degrees.

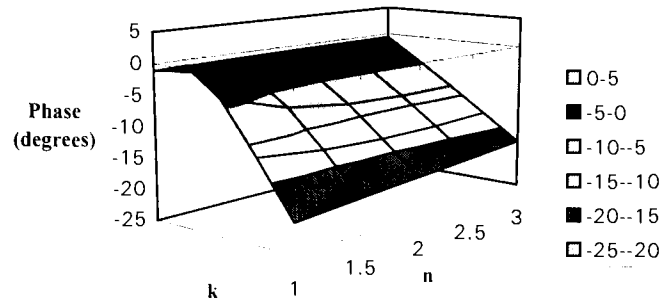

Figure 6: The effect of interface on the change of phase.

Figure 6 is the representation of light passing through the mask substrate, the attenuator and exiting into air. Therefore light passes through two interfaces, first between the fused silica and the attenuator interface, and then the attenuator and air interface. From Figure 6, it can be seen that if materials with high extinction coefficient and low refractive index are used the interface has a significant contribution to the phase change. Therefore, the contributions of the interface to the phase change have to be accounted for when manufacturing an APSM.

Therefore, the true phase change of the light is

$$\phi = \Delta\phi_{absorber} + \Delta\phi_{shifter} + \Delta\phi_{interface}$$

The first term represents the change in the phase due to the light passing through the absorber, the second term is phase change caused by the shifter, and the third term is the effect of the interface. The first two terms can be combined into one if a single layer is used for both phase shifting and attenuation. The quality of the image obtained by using APSM's is strongly dependent on the phase change. Usually the maximum allowed phase

deviation is 5^0. Therefore knowledge of the phase change is critical. The effect that phase error has on the image quality is illustrated in Figure 7, which is a simulation performed on PROLITH, a lithographic simulation program.

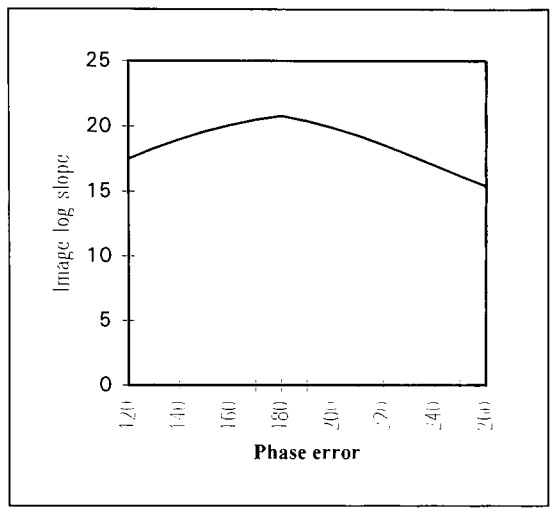

Figure 7: The effect of phase error on the image log slope.

It can be seen from Figure 7 that deviations from the 180^0 phase difference reduces the image log slope. In some extreme cases it is possible to obtain worse images through the use of an APSM than through a chrome on glass mask. Generally this problem can be attributed to poor mask quality for the APSM. Another parameter affecting the performance of an APSM is the transmission through the dark areas. If the transmission is too high then the image contrast is lost, and if it's too low the effect of the phase change becomes negligible. Figure 8, also obtained by using PROLITH, illustrates this fact.

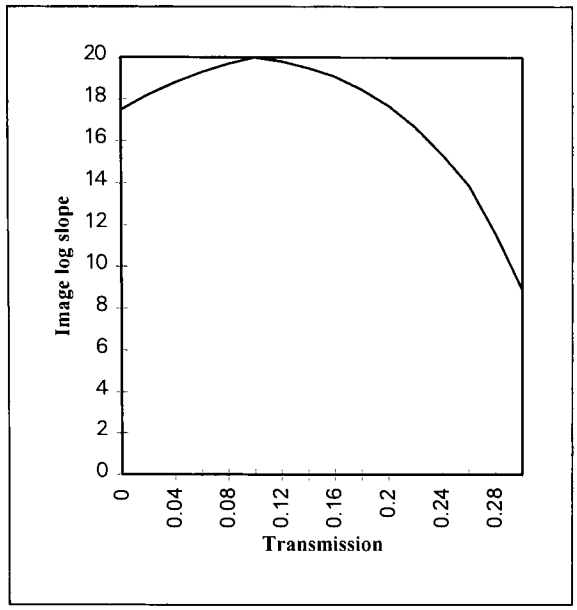

Figure 8: The effect of transmission on the image log slope.

It can be seen from Figure 8 that an APSM with 30% transmission performs the same as a mask with zero transmission or a binary mask. At this point it is important to mention that these simulations were performed for an aberration free ideal lithographic system. In real systems transmission and phase deviations of the magnitude shown in Figures 7 and 8 would lead to catastrophic results. Therefore refractive index (n) and extinction coefficient (k) determines the phase shift and transmission. They need to be measured accurately for any material that is to be used in fabricating an APSM.

2.2 Determination of n and k

There are several techniques for measuring n and k, such as multiple angle or multiple wavelength ellipsometry. A somewhat cheaper technique is through the measurement of normal incidence reflectance and transmission at multiple wavelength. This technique uses the Fresnel and the transmission equations to determine n and k. For a thin film sputtered onto a thick substrate, the normal incidence reflectance and transmission are measured, and n and k values are extracted from this data. The tools required for extracting n and k through this technique are a UV-Visible

spectrophotometer, a method to measure film thickness and an algorithm that extracts the optical constants from the transmission and reflectance data.

2.3 Types of APSM

There are two fundamental types of APSM namely the embedded and the non-embedded type. The difference between these types, is that an embedded APSM is composed of a single material that is responsible for both the phase change and attenuation. Whereas in the non-embedded scheme there are two components each performing a separate function, one layer is responsible for phase change and another attenuates. Generally material selection for the non-embedded scheme is easier whereas it is harder to find materials that will shift the phase and attenuate the intensity of light at the same time. However, embedded type phase shift masks are easier to manufacture since they do not require separate deposition and etch steps. On the other hand, non-embedded type phase shift masks are a good vehicle to verify the concept of phase shifting. Several investigators have done that in the past. The results of their experiments are described briefly. These examples will also demonstrate the process related problem that can be encountered during mask manufacturing, especially for a non-embedded type APSM.

2.3.1 SOG Bi-layer PSM

This mask was fabricated by thinning the chrome of a conventional mask till a transmission of about 8% was obtained. Then a thin layer of SOG was spin coated such that 180^0 phase shift was obtained. After e-beam exposure the SOG was etched in a HF solution, followed by wet etch of Cr. Due to the complex process several problems were reported namely thickness variation of the chrome due to non-uniform etching and undercutting of the SOG due to an extremely high etch rate of the SOG [7].

2.3.2 Etched quartz Cr-APSM

A thin layer of chrome was sputtered and patterned. To obtain a 180^0 phase shift the fused silica of the mask substrate was dry etched. The surface roughness of the fused

silica was measured using an AFM, it was observed that the surface had a thickness variation of about 100 A that corresponds to a phase error of about 9.4^0. To reduce the surface roughness the mask was dipped in dilute HF. This process reduced the variation to about 20 A. The major problem associated with this method was the lack of thickness control during the etch process [8].

2.4 Requirements for an embedded APSM

The obvious requirements for an APSM are 180^0 phase shift and 5-10% transmission. Any stray light in the optical system can degrade the image quality, therefore mask reflectivity is also a concern, it is desirable to have a reflectance of less than 15% at exposure wavelength. For an APSM most of the reflected light is due to front surface reflectance, this is because of the transmission requirements placed on this type of mask. The front surface reflectance can be calculated using the Fresnel equation. High values of n and k can lead to higher reflectance as illustrated in Figure 9.

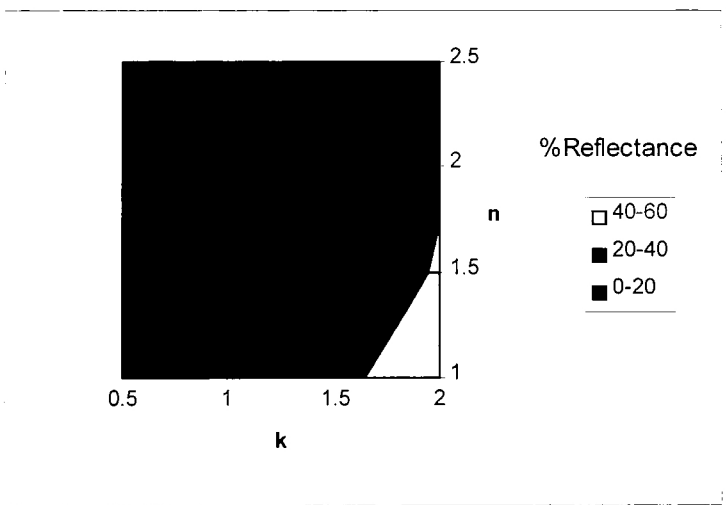

Figure 9: Effect of high values of refractive index (n) and extinction coefficient (k) on reflectance.

Another concern is transmission at alignment wavelength. It is desirable to have transmission less than 40% at 488 nm, which is the wavelength currently used for alignment. Since transmission is an inverse exponential function of wavelength, the extinction coefficient at 488 nm has to be much larger than at 193 nm to obtain the same transmission.

In the past pattern transfer on the mask was performed using wet chemical etching, this technique was feasible at longer wavelengths because the feature size was large. For the feature sizes at 193 nm wet etching would not be feasible because the feature size would be comparable to the film thickness. Therefore, dry etching would have to be used, which means that the material has to be selectively etched with respect to fused silica and resist. Also since mask fabrication requires electron beam exposure the mask material has to be conductive to prevent charging up of the resist. Another issue is the stability, the material should not change after exposure to 193 nm radiation and it should be relatively insensitive to chemical reagents used for mask cleaning.

2.5 Possible materials for 193 nm APSM

The primary criteria for selecting a material are the refractive index and the extinction coefficient of the material at 193 nm. The optical constants of a material are dependent upon the atomic structure and the behavior of the electrons in the lattice. Several theories have been postulated to describe the optical characteristics of a material.

2.5.1 Free electron theory

In this theory it is assumed that the electrons are free to move without any sort of damping, in essence a perfect lattice. The value of the electric field of a plane polarized light is given by [9]:

$$E = E_0 \exp(i\omega t)$$

where $\omega = 2\pi\nu$ is the angular frequency, t is the time and E_0 is the maximum value of the electric field. The force exerted on the electron by this electric field is $e\varepsilon$, therefore the one dimensional equation of motion becomes

$$m \frac{d^2x}{dt^2} = eE$$

where m is the mass of the electron. The displacement of the electron is solution of this equation,

$$x = -\frac{eE}{4\pi^2 m\nu^2}$$

The vibrating electron can be considered as a dipole. The dipole moment of the electron would be the product of the displacement of the electron and the charge. The polarization P is the total dipole moment per unit volume or exN_f. The dielectric constant is defined as

$$\varepsilon = 1 + \frac{4\pi P}{E}$$

therefore,

$$\varepsilon = 1 - \frac{e^2 N_f}{\pi m\nu^2}$$

also,

$$\varepsilon = n^2 - k^2 - i2nk$$

From the above relations it can be seen that the free electron theory would predict that the reflectance R would be very high at low frequencies and at higher frequencies it would be

$$R = \frac{(n-1)^2}{(n+1)^2}$$

2.5.2 Free electrons with damping and bound electrons theories

The free electron theory is not sufficient to account for the optical behavior of the various materials. To more accurately describe a real system, the collisions of the electrons with the atoms of a non-ideal lattice have to be accounted for. The following relation introduces a damping term to account for lattice collisions

$$m \frac{d^2x}{dt^2} + \gamma \frac{dx}{dt} = eE$$

where γ is called the damping coefficient. Under a constant electric field $dx/dt = v_d$ the drift velocity, which is proportional to the conductivity σ of the material. Since

$$v_d = \frac{\sigma E}{eN_f}$$

and also

$$v_d = \frac{dx}{dt} = \frac{eE}{\gamma}$$

therefore

$$\gamma = \frac{e^2 N_f}{\sigma}$$

If the electrons are bound, the electric field merely displaces the electron cloud around the nucleus of the atom. This implies a spring like behavior that can be described by F = Kx, where K is a proportionality constant. Taking this additional force into account the equation of electron motion becomes

$$m\frac{d^2x}{dt^2} + \gamma\frac{dx}{dt} + Kx = eE$$

The solution of the above equation is

$$x = \frac{eE\exp\{i(\omega t - \phi)\}}{\sqrt{[m2(K/m - \omega^2)^2 + \gamma^2\omega^2]}}$$

where

$$\phi = \tan^{-1}[\gamma\omega/(m(K/m - \omega^2)]$$

Therefore the dielectric constant becomes,

$$\varepsilon = \frac{4\pi e^2 N_a \exp\{i((\omega t - \phi)\}}{\sqrt{[m^2(K/m - \omega^2)^2 - \gamma^2\omega]}}$$

where N_a is the number of dipoles per unit volume, K/m is the resonant frequency of the oscillator. Since $\varepsilon = n^2\text{-}k^2\text{-}i2nk$, the refractive index and the extinction coefficient can be extracted from the above equation. By combining the free electron theories and the bound electron theory the optical behavior of material can be explained with reasonable accuracy.

Other material properties that have to be taken into account before selecting a material are transmission at alignment wavelength, dry etch capability and material stability. Transmission at alignment wavelength depends on the extinction coefficient of the material at alignment wavelength. The dry etching of a material is dependent on its

capacity to form volatile compounds. However, the optical constants at 193 nm are the primary selection criteria.

2.6 Sputter deposition

Sputtering is a thin film deposition technique that is commonly used in the electronic industry. Figure 10, is a schematic of a sputtering system.

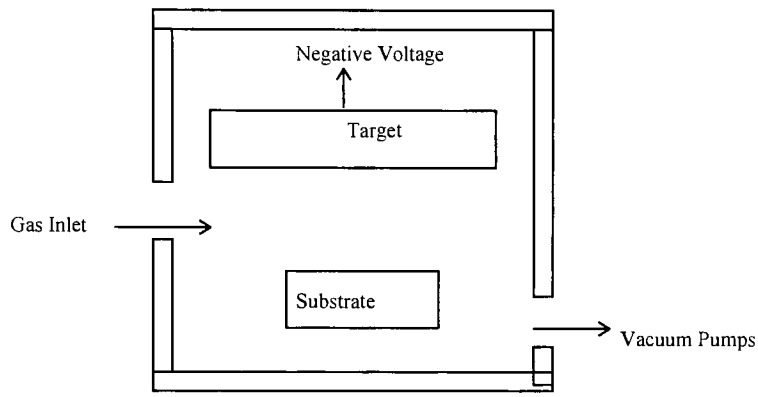

Figure 10: Schematic of a typical sputtering system.

Typically, the material that has to be deposited (target)is connected to a negative voltage supply [10, 11, 12]. The substrate holder faces the target. The substrate holder could be grounded, floating, biased, heated, cooled or some combination of these. A gas is introduced to serve as a medium in which a glow discharge can be initiated and sustained. Argon is the most common sputtering gas. Typical pressure inside the chamber ranges from a few mTorr to 100 mTorr.

When the glow discharge is started, positive ions strike the target plate and remove target atoms by momentum transfer these atoms condense into thin films on the substrate and the chamber walls. In some cases, gas mixtures are used. This involves some sort of reactive sputtering in which a compound is formed by sputtering a metal target in the presence of a reactive gas e.g. TiO_2, by sputtering Ti in the presence of Ar and O_2.

2.7 Dry Etching

The viability of a material also depends upon whether the film can be dry etched. Dry etching is similar to sputtering, it is performed under reduced pressures and a plasma is used to generate excited species that enhance the etching process. A reaction that would otherwise require elevated temperature can be performed at lower temperatures during dry etching [12]. In an etching system the substrate is placed at the cathode the ionized gas atoms are attracted to the substrate and hence enhance the etching process by bombarding the substrate surface. Parameters of concern while dry etching are selectivity, anisotropy and etch rate. An optimum etch process would be extremely selective, fast and extremely anisotropic. To meet the conditions described above gas chemistry, power and pressure can be adjusted.

3.0 Experimental

Several materials were investigated, the following section summarizes the initial selection criteria and techniques used for depositing, analyzing and etching these materials.

3.1 Material screening

As mentioned earlier the primary selection criteria were the optical constant at 193 nm. The values of these constants were obtained from an extensi- literature search. Figure 11 is a plot of n and k values for various materials at 193 nm.

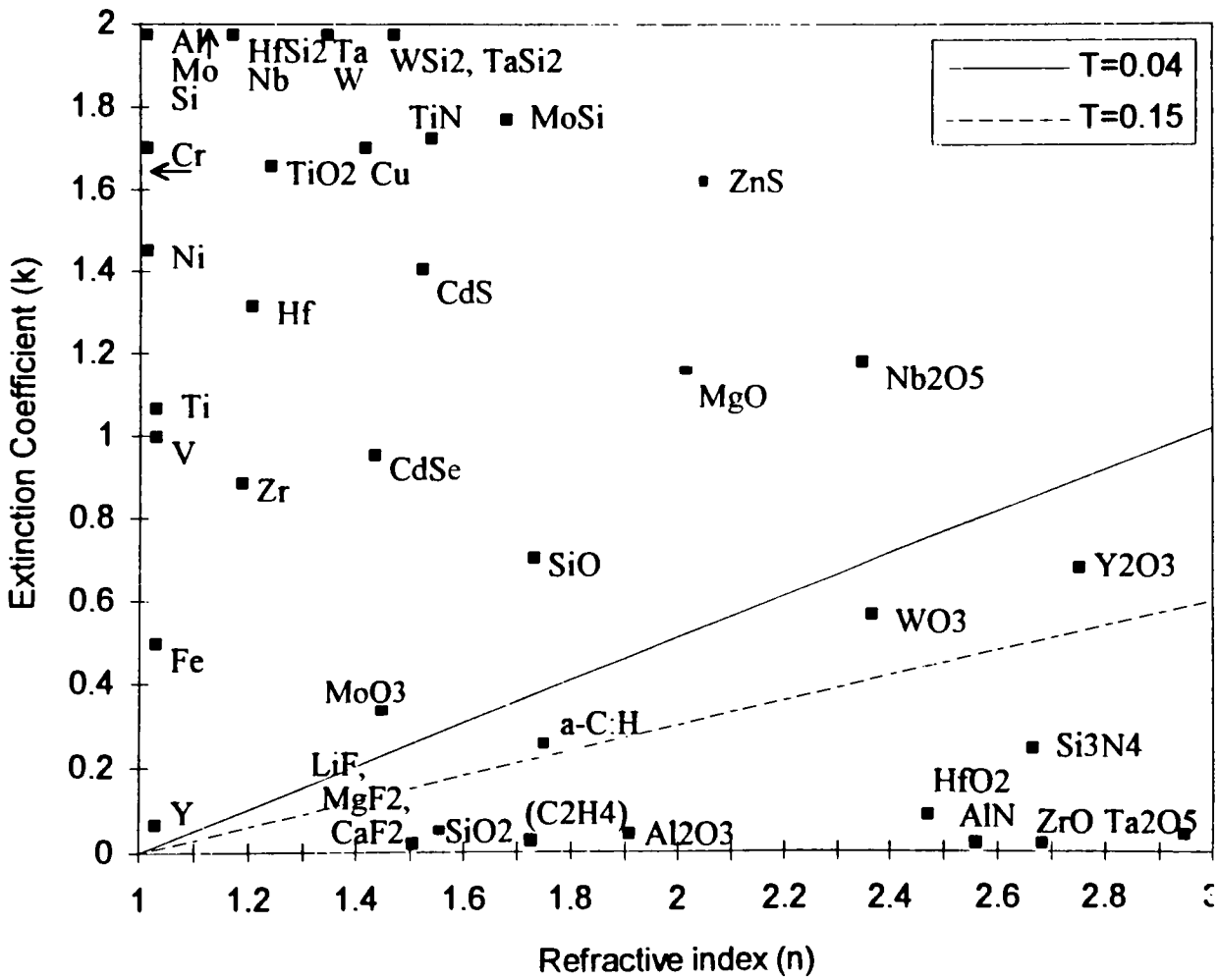

Figure 11: n and k values of various materials at 193 nm.

The wedge in Figure 11 indicates the n and k values that could give a 180^0 phase shift and transmission between 4 and 15%. Values at either extreme are undesirable. Materials with low n values would require extremely thick film. Materials with high n values on the other hand would require very thin films. These films could have continuity problems as well high reflectance as mentioned before. It is obvious from Figure 11 that very few materials fall within this wedge; WO_3 is extremely transparent at alignment wavelength, Y_2O_3 cannot be etched, a:C is unstable and changes after prolonged exposure to 193 nm. However, it may be possible to combine materials that would not be the obvious choice to obtain the desired optical properties. By selecting the individual components carefully it may be possible to tailor the optical and the physical properties of the material.

3.2 Deposition

Films were deposited onto clean dehydrated fused silica pieces so that the optical constants could be extracted. For film deposition Perkin Elmer 2400 and CVC 601 sputtering systems were used.

3.2.1 CVC 601 system

The 601 is a sputter up system. It can be used in DC or RF modes. The ultimate base pressure that can be achieved in this system is ~2E-6 Torr. A Brookes mass flow controller is used to regulate the gas flow. The system has to be tuned manually and the film is deposited onto a rotating substrate. The system also has a substrate heater available that can be used to heat the substrate to about 300^0C.

3.2.2 PE 2400 system

This system is a sputter down system. It can be used in RF mode only. The ultimate base pressure of this system is ~1E-7 Torr. This system like 601 also uses a Brookes mass flow controller. The system is set up for tuning itself automatically. This system can be used to deposit on a rotating substrate or a stationary substrate. If the

stationary substrate mode is used four films can be deposited in one pump down. All films but the Molybdenum silicon oxide were deposited in the 2400.

3.3 Etching

A PlasmaTherm 2000 system was used for etching the films after they had been optically analyzed. A portion of the film was masked and the etch rate was measured using a profilometer that was scanned across the unmasked and the masked portion of the film. At the same time a silicon wafer with thermal oxide and a wafer with photo resist were placed inside the etch chamber. This was done to simulate the etch behavior of fused silica and photo resist. A brief description of PlasmaTherm 2000 follows

3.3.1 PlasmaTherm 2000

It is a parallel plate RF etch system. It has inlets for six different gases, all of which can be used at the same time. The power, pressure and gas flows should be adjusted before introducing the substrate into the chamber. The system tunes itself automatically and typical operating pressures are in the range of 10-100 mTorr. To accommodate chlorine based chemistry the system had to be especially modified.

3.4 Optical analysis

A Perkin Elmer UV-visible spectrophotometer was used to obtain reflectance and transmission spectra. The working principle of this system is described below, as well as the method used for extracting n and k information from transmission and reflectance spectra.

3.4.1 Spectrophotometer

Spectrophotometer is a device that measures the transmission and reflectance of a material over a range of wavelength. The Perkin Elmer Lambda 11 spectrophotometer has a wavelength range of 900 nm to 190 nm. A tungsten lamp is employed from the near infrared (900 nm) to the near UV (320 nm) , and for the remainder of the wavelength

range a Deuterium lamp is used. The following figure is the schematic of a spectrophotometer.

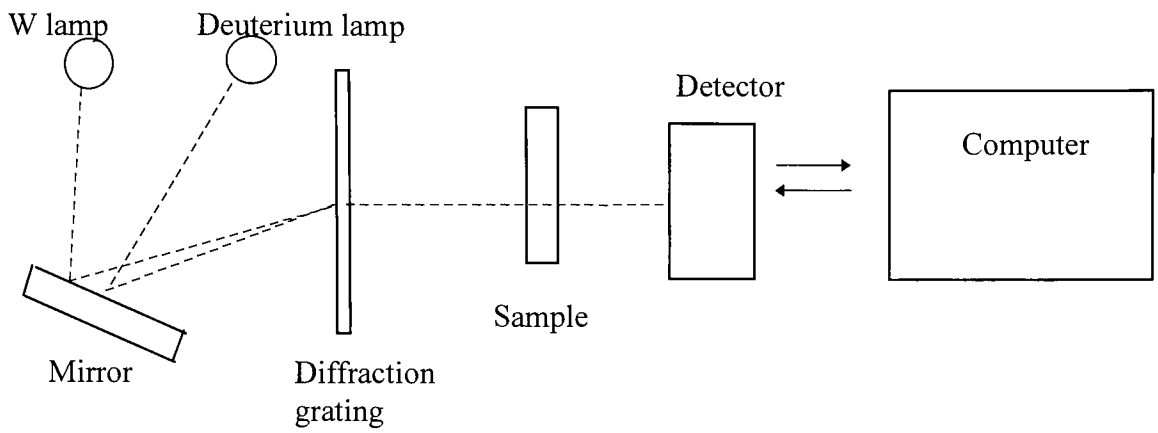

Figure 12: Schematic of a spectrophotometer.

Both lamps emit their entire range of wavelengths at all times. A diffraction grating is used to separate the emission spectra into its components. A reference measurement has to be made before measuring the sample. The reference for transmission measurements is air and for reflectance it's a standard whose reflectivity is known over the entire wavelength range.

3.4.2 Extraction of n and k

A commercially available software package was used for extracting the optical constants from the transmission and reflectance data. This program solves Fresnel and transmission equations to determine the n and k values from the reflectance and transmission spectra. Figure 13 illustrates some of the parameters that are utilized for the extraction of n and k.

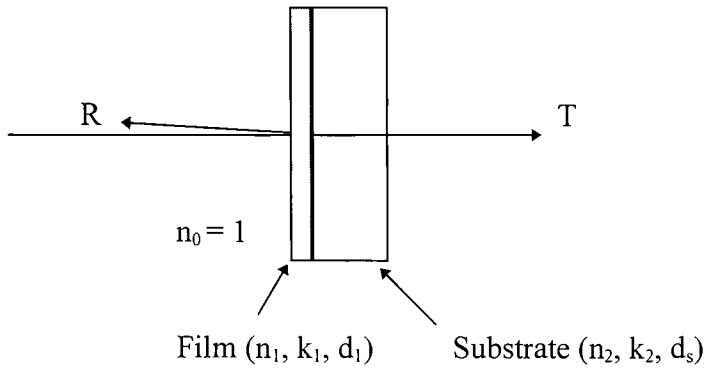

Figure 13: Parameters used for extracting n and k.

The light passes through air that has an index of n_0, and an extinction coefficient of zero. It then passes through the thin film that has an index of (n_1,k_1) and the film thickness is d. It is assumed that d is small enough that interference fringes are produced within the film. The film is generally deposited onto a substrate that has an index of (n_2, k_2) and a thickness of d_s. It is assumed that the substrate is thick enough to preclude the possibility of coherent reflection. Light emerges from the back of the substrate into air where the transmission T is measured, the reflectance R is measured on the front side. Hence, given n_0, n_2, k_2, d and d_s and the observed reflectance and transmission measurements over the entire wavelength range, the optical constants have to be extracted. This is done by solving the Fresnel equation and the transmission equation iteratively through the entire wavelength range. The results obtained can then be verified by generating a reflectance and transmission spectra from the extracted n and k values.

3.5 Film stability analysis

Some materials were exposed to 193 nm radiation to observe the effects of prolonged 193 nm radiation exposure. The films were tested on a Lumonics EX700 ArF excimer laser. They were subjected to energy levels corresponding to 1X, 10X and 100X of the expected irradiance level at the mask plane. This corresponds to 8 mW/cm^2, 80 mW/cm^2, and 800 mW/cm^2 on the mask plane. Typical irradiance level at the wafer plane is expected to be 200 mW/cm^2 for a 5X reduction exposure system. Testing was

performed to simulate 10,000 8" wafers, assuming a resist sensitivity of about 20 mJ/cm^2. Due to exposure to the excimer radiation, changes in some films are observed. These changes are either due to thickness changes in the film or there is a change in the stochiometry of the material. The incremental change in transmission was measured after every 25,000 pulses upto 100,000 pulses. Changes in refractive index and extinction coefficient were not extracted. The actual cause for the change in transmission was also not determined.

3.6 Materials

3.6.1 Molybdenum Silicon Oxide

Films based on molybdenum silicide have been looked at by several investigators as a possible replacement for chrome, because it can be dry etched easily. However, molybdenum silicide by itself has a very high extinction coefficient to be of any use for APSM application. It may be possible to get the desired optical properties by using a film composed of some combination of molybdenum, silicon and silicon dioxide as illustrated in the Figure 14.

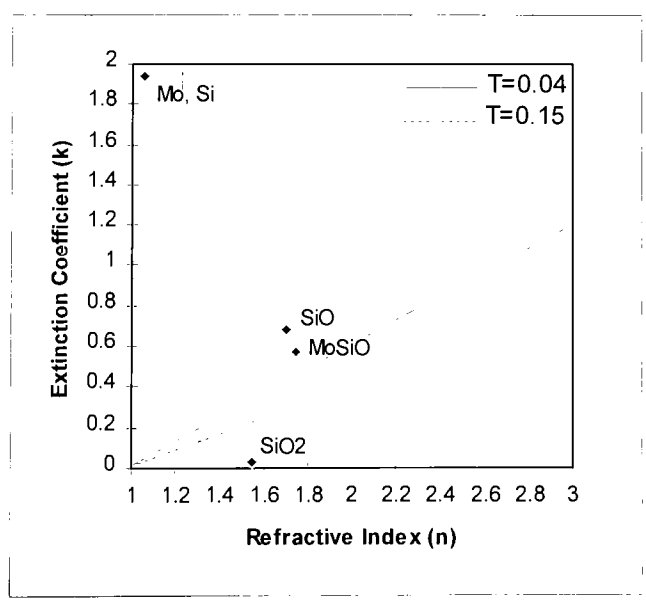

Figure 14: Optical constant for molybdenum and silicon based materials.

Reactive sputtering using oxygen as the reactive gas was used to deposit MoSi-O films in the CVC 601 magnetron sputter system. A mosaic target composed of small pieces of silicon placed on an 8" molybdenum target was used. The amount of silicon chips used were varied to adjust the Si/Mo ratio. Also, the amount of oxygen was varied to obtain a variety of films. The films were deposited at 500 W, with 2% to 6% of oxygen in the gas mix. The reason for using these conditions was to allow for suitable reactivity of the target and at the same time avoid oxidizing the target. The target was pre-sputtered before each run. All films were deposited onto fused silica substrate to allow for optical characterization. The sputter rate of silicon and molybdenum was determined individually and it is described in Table 1

Material	Sputter Rate
Molybdenum	9 A/min
Silicon	15 A/min

Table 1: Sputter rate of molybdenum and silicon.

Based on these rates and early transmission screening experiments, target design that represented Si:Mo ratio of 2.0:1, 2.1:1 and 2.2:1 were chosen. Optical evaluation was performed as described in section 3.4. Similarly the etch evaluation is described in sections 3.3. Table 2 describes the melting points and boiling points of silicon and molybdenum based compounds. This table can be used as a guideline to determine which chemistry to use for etching molybdenum silicon oxide films.

Compound	Melting Point	Boiling Point
$MoCl_5$	194 C	268 C
MoF_6	17.5 C	37 C
$MoOCl_4$	subl.	
$MoOCl_3$	subl.	
$MoOF_4$	98	180

SiO_2F_6	-48	-23
Si_2OCl_6	28	137

Table 2: Physical properties of Mo and Si based materials, from ref 13.

The boiling points and melting points as described in Table 2 were measured at atmospheric pressure, whereas the etching process is carried out under reduced pressure that would reduce the temperatures.

3.6.2 Aluminum/Aluminum Nitride

Aluminum Nitride has a band gap of 6.18 eV that makes it an extremely suitable material. Also as can be seen from Figure 15 by adding sufficient amount of aluminum to the aluminum nitride the optical properties can be tailored to match the requirements for an APSM material.

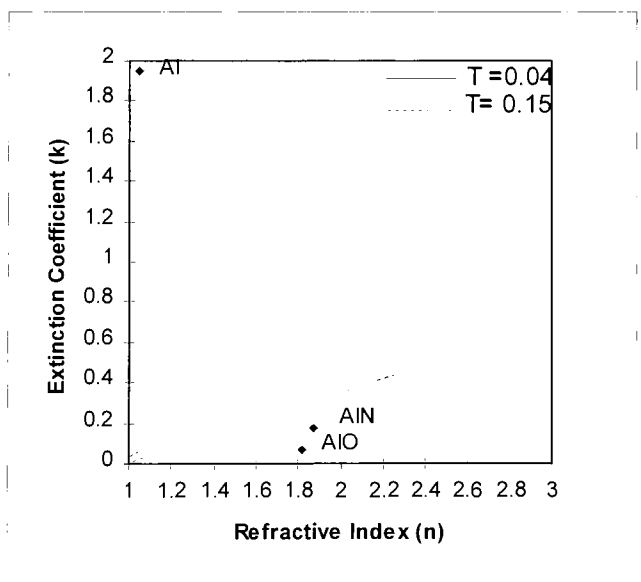

Figure 15: Optical constants of Al based materials at 193 nm.

Films were deposited in the PE 2400 sputterer using an 8" (99.999%) aluminum target in a gas mixture of argon and nitrogen. 500W of power was used to deposited the

films, the base pressure of chamber was 1E-7 Torr. Once again the films were deposited onto clean dehydrated fused silica plate. The flow rates of argon and nitrogen were controlled to vary film composition. Films were deposited without substrate heating. Optical and etch evaluations were carried out in a similar fashion as described in sections 3.4 and 3.3 respectively. Fluorine based chemistry is not suitable for etching aluminum since AlF_3 has a very low vapor pressure (100 Torr at 1400 C). Other halides of aluminum have higher vapor pressure ($AlCl_3$: 100 Torr at 150 C). Ion bombardment is required to assist in the etching process of aluminum.

3.6.3 Under-Stoichiometric Silicon Nitride

Several investigators have looked at silicon nitride as an APSM material for the 248 nm regime. By using under-stoichiometric silicon nitride it may be possible to produce the desired optical properties. Also since silicon nitride is used extensively in the microelectronic fabrication process, a lot of information is available on this material. The optical properties of silicon nitride can be tailored by adding silicon to obtain the desired results as illustrated in Figure 16.

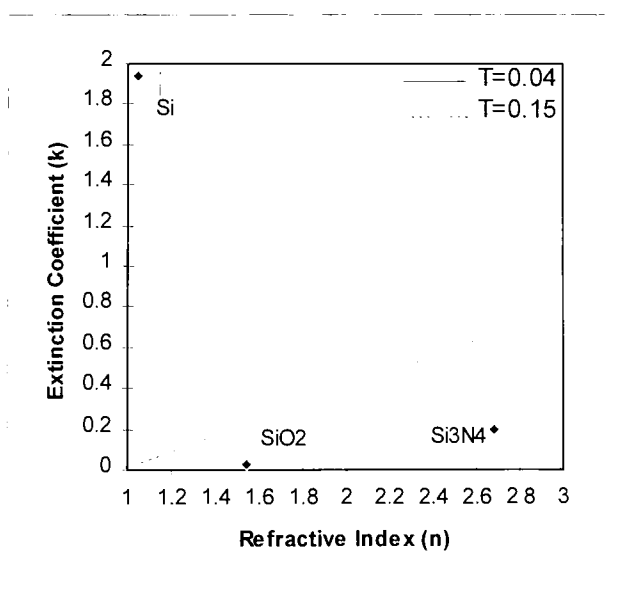

Figure 16: Optical constants for Si based compounds at 193 nm.

Silicon nitride films were deposited from a silicon target in the PE 2400, in the presence of argon and nitrogen. Typical power used in the deposition process was about 500W. The partial pressure of argon and nitrogen were varied to obtain the desired results. Optical evaluation was performed as described in section 3.4. Since silicon nitride is used extensively in the microelectronic industry the etch behavior of silicon nitride was not studied extensively.

3.6.4 Silicon Nitride/Zirconium multilayer

Zirconium nitride is a very stable material, combining it with silicon nitride may lead to some interesting results. Since it was not possible to co-sputter these materials it was decided to layer them by depositing extremely thin films of one material followed by the other. Another advantage of layering is that the stochiometry of each component can be controlled exactly which leads to better understanding of the film behavior.

Silicon nitride was deposited as described in section 3.2.3. Zirconium nitride was deposited from a (99.999%) zirconium target in the PE 2400, in the presence of nitrogen and argon. This time the power levels were varied from 500W to 1300W to optimize the composition of zirconium nitride, the rationale behind this approach was that the zirconium nitride would provide the metallic component of multilayer. Instead of using an under-stoichiometric material, layers of stoichiometric materials were deposited. Zr-halides such as dichlorides, trichlorides and tetrachlorides have moderate melting points (350-450 C). Bromine based compounds also have moderate melting/boiling points. Also, zirconyl chloride has a boiling point of 210 C, which may provide another avenue for etching Zr-based films in a Cl-based etch chemistry.

4.0 Results

4.1 Molybdenum Silicon Oxide

4.1.1 Deposition and Optical characterization

Initially several films of MoSi-O were sputtered to get an idea of the refractive index and extinction coefficient at 193nm. It was believed that a significant portion of the deposited film is molybdenum oxide (MoO_3), therefore several films were deposited from an oxidized molybdenum target. Figure 17 shows the refractive index and the extinction coefficient of a MoO_3 film. It seems that MoO_3 would be suitable for use as an APSM material at 193nm, however the film becomes extremely transparent above 400nm making it unsuitable for alignment and inspection at visible wavelengths.

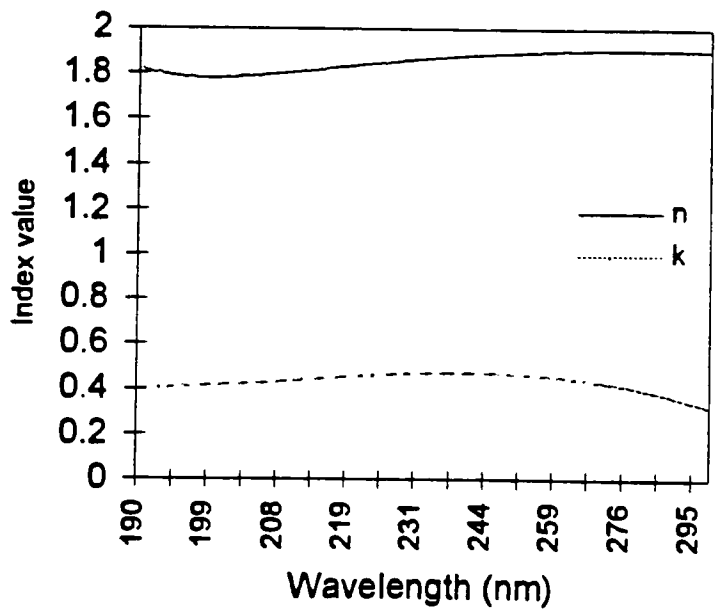

Figure 17: The refractive index and the extinction coefficient of MoO_3 as a function of wavelength.

A series of MoSi-O films was deposited. The silicon to molybdenum ratio was varied as well as the oxygen partial pressure. The silicon to molybdenum target area ratio

was varied to obtain a deposition rate of 2.0:1, 2.1:1 and 2.2:1 of Si:Mo. The oxygen partial pressure was varied by adjusting the flow rate of the individual gas. The oxygen flow rate was varied from 3sccm to 5sccm, while keeping the argon flow rate at 100sccm. This corresponds to partial pressures of 2.91%, 3.85% and 4.76%. The extracted n and k values are shown in Figure 18. The results are summarized in Table 3.

Si:Mo/ O2 partial press.	Ref. Indx @ 193nm	Extinct Coeff @ 193nm	Thickness for 180 phase shift (um)	Transmission @193 nm for d(180,193)	Extinct Coeff @ 500nm	Transmission @ 500 nm for d(180,193)
	n(193)	k(193)	d(180-193)	T(180-193)	k(500)	T(500)
2/4.76%	1.52	0.28	0.1856	0.0339	0.028	0.8776
2.1/4.76%	1.44	0.117	0.2193	0.1881	0.016	0.9156
2.2/4.76%	1.46	0.06	0.2098	0.4406	0.001	0.9947
2/3.85%	1.75	0.52	0.1287	0.0128	0.07	0.7974
2.1/3.85	1.84	0.623	0.1149	0.095	0.099	0.7514
2.2/3.85	1.63	0.26	0.1532	0.0748	0.065	0.7786
2/2.91%	1.99	0.766	0.0975	0.0077	0.3	0.4795
2.1/2.91%	1.912	0.623	0.1058	0.0137	0.28	0.4749
2.2/2.91%	2.08	0.54	0.0894	0.0432	0.275	0.5393

Table 3: Summary of the optical constants for MoSi-O films.

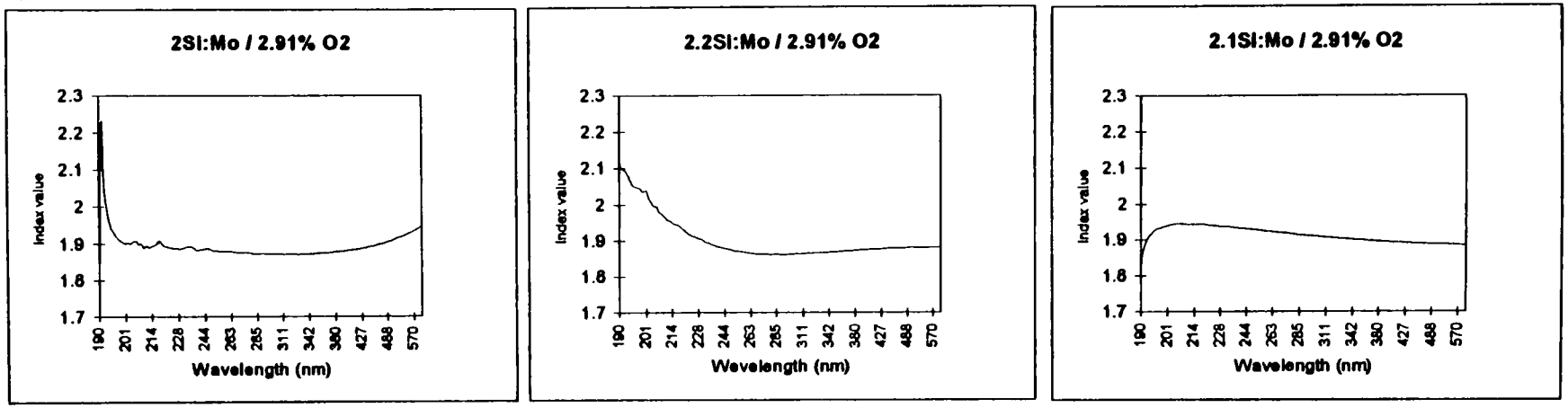

Refractive Index (n) - 2.91% O_2 in Ar series

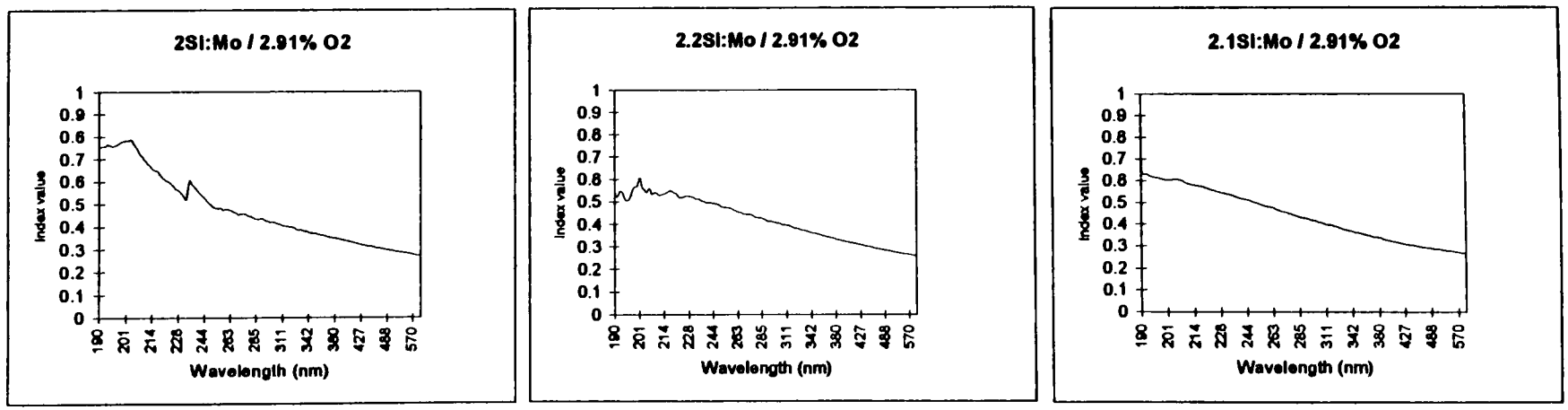

Extinction Coefficient (k) - 2.91% O_2 in Ar series

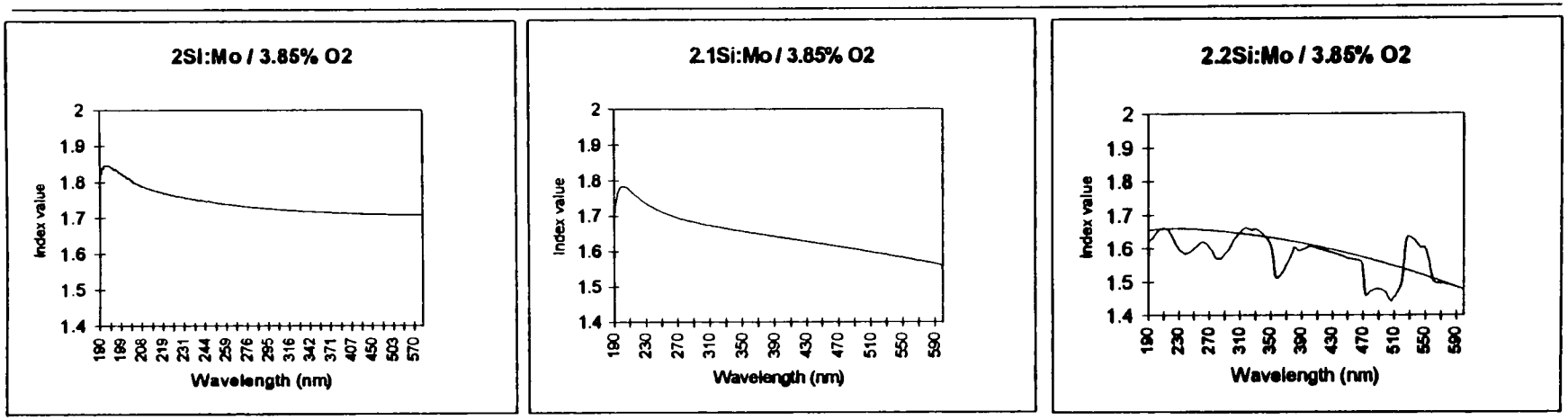

Refractive Index (n) - 3.85% O_2 in Ar series

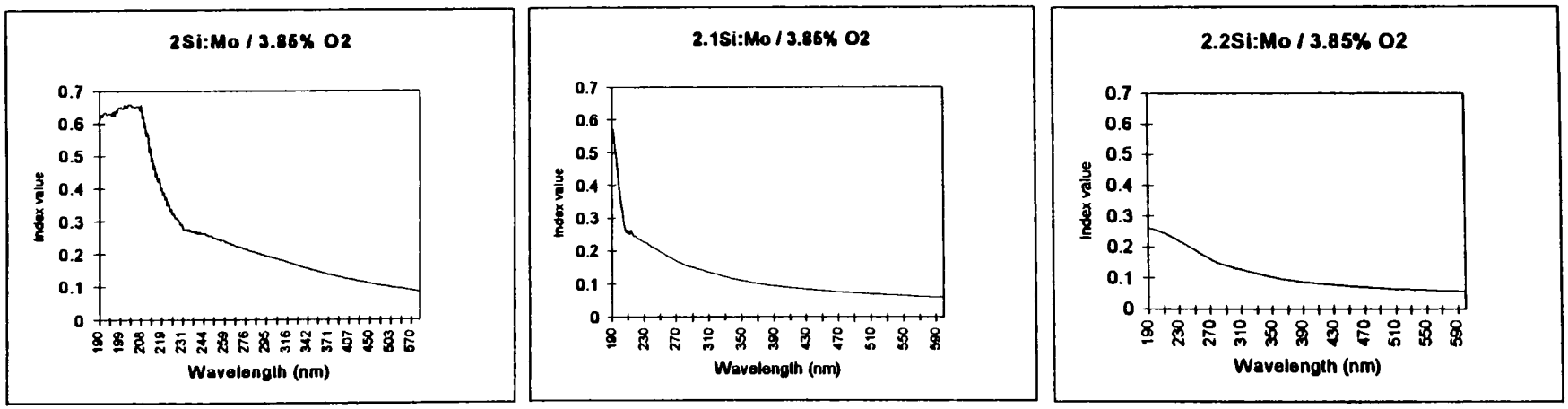

Extinction Coefficient (k) - 3.85% O_2 in Ar series

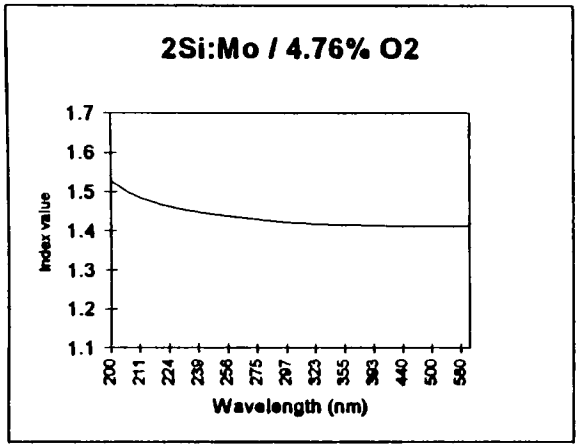

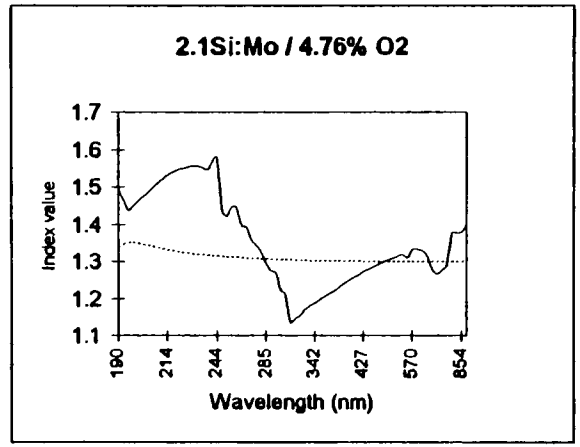

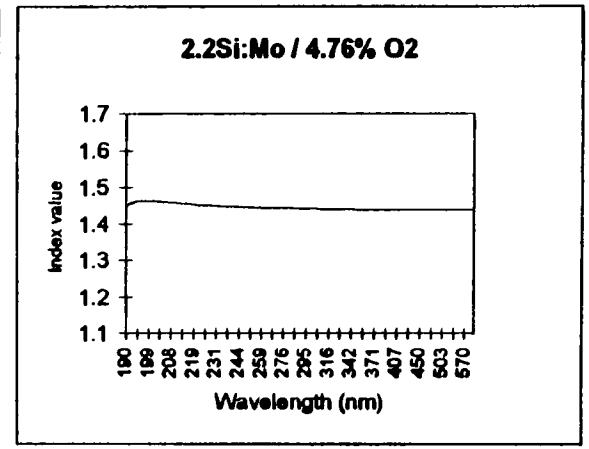

Refractive Index (n) - 4.76% O_2 in Ar series

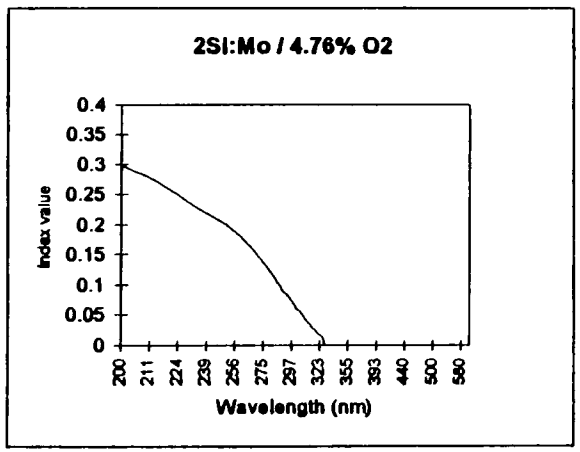

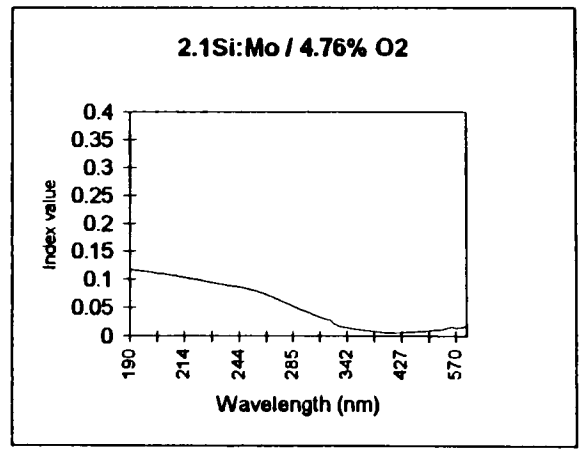

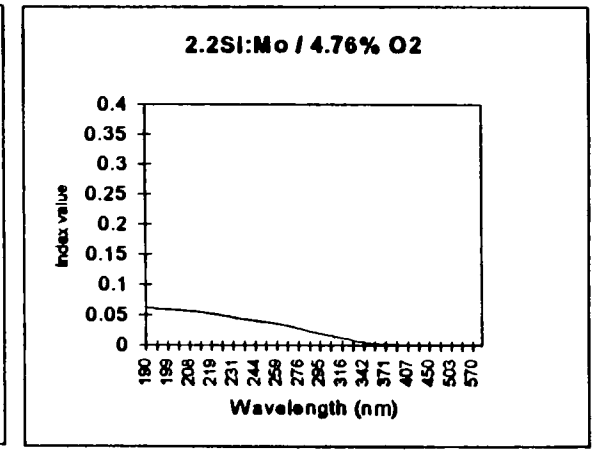

Extinction Coefficient (k) - 4.76% O_2 in Ar series

Regression analysis was performed on the results. Figure 18 is the graphical representation of the model that describes the behavior of the film as the oxygen flow rate and the silicon to molybdenum target ratios are varied. As is obvious from these figures, the refractive index is somewhat independent of the Si:Mo target ratio but is dependent on the oxygen flow ratio. However, the extinction coefficient is dependent on both Si:Mo ratio and oxygen flow rate. Several optimizations were performed on the MoSi-O deposition. Table 4 summarizes the results of the these optimizations.

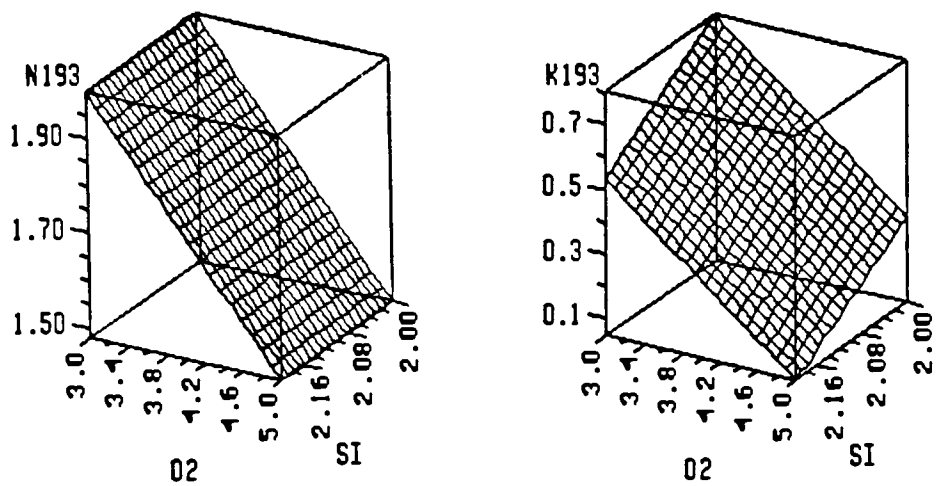

Figure 19: Graphical representation of the effect of Mo/Si ratio and oxygen flow on the refractive index and extinction coefficient of MoSi-O at 193nm.

For a 4% transmitting film	*For a 10% transmitting film*
Si:Mo=2.2:1 ; 3.4% O2	Si:Mo=2.2:1 ; 3.8% O2
T(500nm) = 68%	T(500nm) = 81%
Film thickness = 1165 A	Film thickness = 1400 A

Table 4: Film characteristics for an optimized MoSi-O film.

4.1.2 Etching

Several plasma chemistries were identified which could be used to pattern the MoSi-O film. The results of these investigations are listed in Table 5.

SF6 + O2 process	*CF4 + O2 process*
SF6 = 50sccm	CF4 = 50sccm
O2 = 5sccm	O2 = 2.5sccm
30mT, 100W	30mT, 100W
MoSi-O etch rate = 600A/min	MoSi-O etch rate = 90A/min
Selectivity to fused silica = 2.14:1	Selectivity to fused silica = 1.5:1
Selectivity to Novolac = 0.6:1	Selectivity to Novolac = 0.6:1

Table 5: Etch data on the MoSi-O films.

As is obvious the etch process has not been optimized. Furthermore anisotropy was not investigated. This optimization should be performed before implementing this material into a manufacturing environment.

4.2 Aluminum/Aluminum Nitride

4.2.1 Deposition and Optical Characterization

Deposition parameters for films were varied as show in Table 6, which resulted in a range of optical properties. The deposition parameters were varied to achieve high quality films that met the optical requirements for 193nm APSM.

Series No.	Sample No.	Power (W)	N_2 flow (sccm)	Ar flow (sccm)	Deposition (min)
I	51226B	500	20	15	60
	60112A	500	15	15	60
	51224A	500	10	15	60
	51225A	500	5.0	15	60
	60116B	500	4.0	15	60
	51229A	500	3.0	15	60
	60113A	500	2.9	15	60
	51230A	500	2.8	15	60
	60115A	500	2.7	15	60
	51226A	500	2.5	15	60
II	60119A	500	1.5	20	60
	60122B	500	1.5	20	40
	60119B	500	1.5	25	30
	60122A	500	1.5	15	20
III	60123A	500	2.0	15	20
	60123B	500	2.5	15	20
	60123C	500	3.0	15	20
IV	60125A	500	3.0	20	20
	60125B	500	3.5	20	20
	60125C	500	4.0	20	20
	60126A	500	3.1	20	20
	60126B	500	3.2	20	20
	60126C	500	3.3	20	20
	60126D	500	3.4	20	20

Table 6: Sputter conditions for AlN films.

Figure 19 shows the transmittance and reflectance for a pure AlN film. The film thickness is 3940 A. As is obvious the transmission of this material is quite low at wavelengths below 200nm but remains quite high at wavelengths in the visible regime. Therefore stochiometric AlN is not suitable as an APSM material because of its low absorption in the visible region. However, since stochiometric AlN has a band gap of about 6.18 eV, it has useful optical properties in the UV regime.

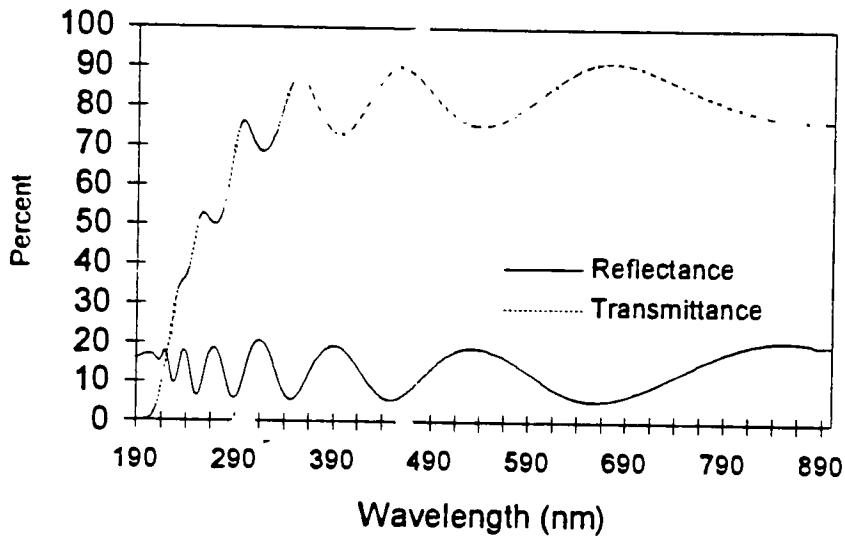

Figure 20: The transmission and reflectance spectra of pure stochiometric AlN.

It may be possible to modify the optical properties of AlN in the visible region by adjusting the depostion parameters, essentially modifying the material. Figure 20 shows the transmission spectra of three flims, these films were sputtered under reduced nitrogen partial pressure, which leads to aluminum rich films. However, these films are still too transparent in the visible region. Figure 21 is the reflectance spectra of the same films.

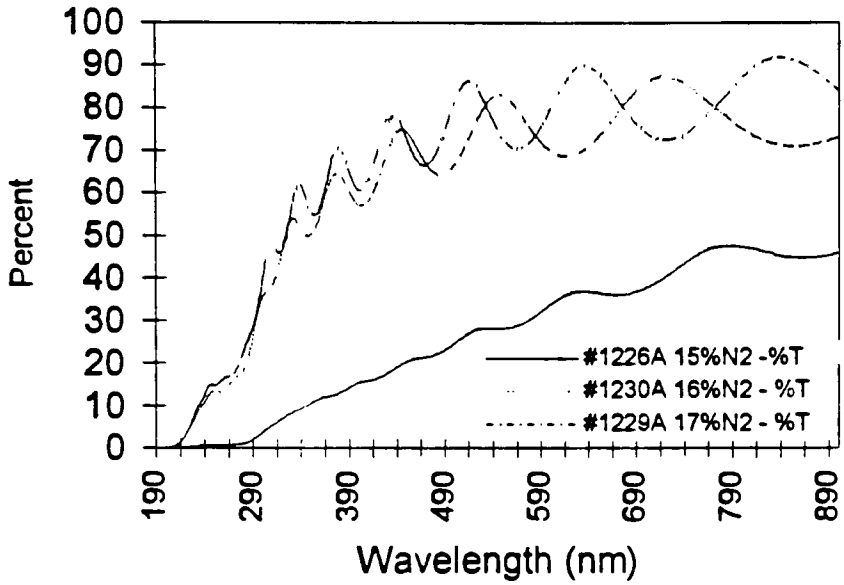

Figure 21: Transmission spectra of under-stochiometric AlN films

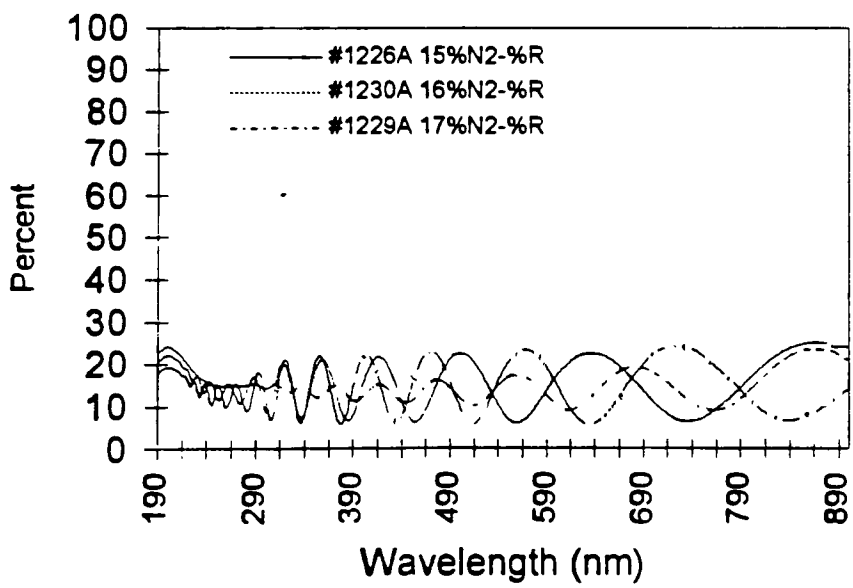

Figure 22: Reflectance spectra of several under-stochiometric AlN films

Series IV films were deposited at Ar flow of 20sccm with N_2 flows of 3.0 to 4.5 sccm, corresponding to 13.0 to 18.4% partial pressure of N_2. Transmission in the visible region for these films was low enough to make them suitable for APSM application. The transmission and reflectance spectra of these films are shown in Figure 22 and Figure 23 respectively. Corresponding film thicknesses are listed in Table 7.

Sample No.	$\%N_2$	Thickness
60125A	13.0%	1545A
60126A	13.4%	1500A
60126B	13.7%	1700A
60126D	14.5%	1720A
60125B	14.9%	1600A

Table 7: Thickness data for series IV films.

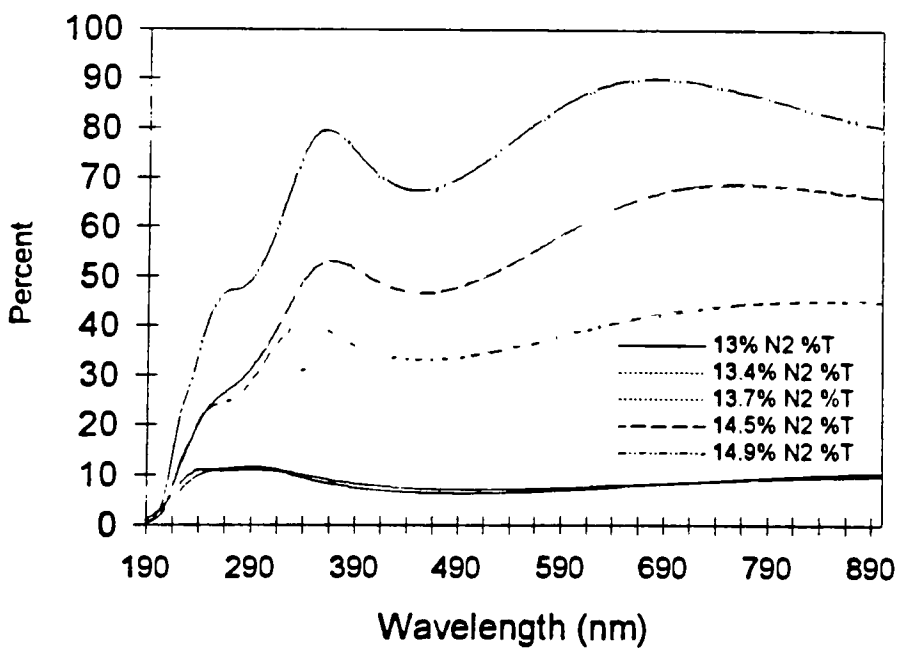

Figure 23: The transmission spectra of a series of under-stochiometric AlN film

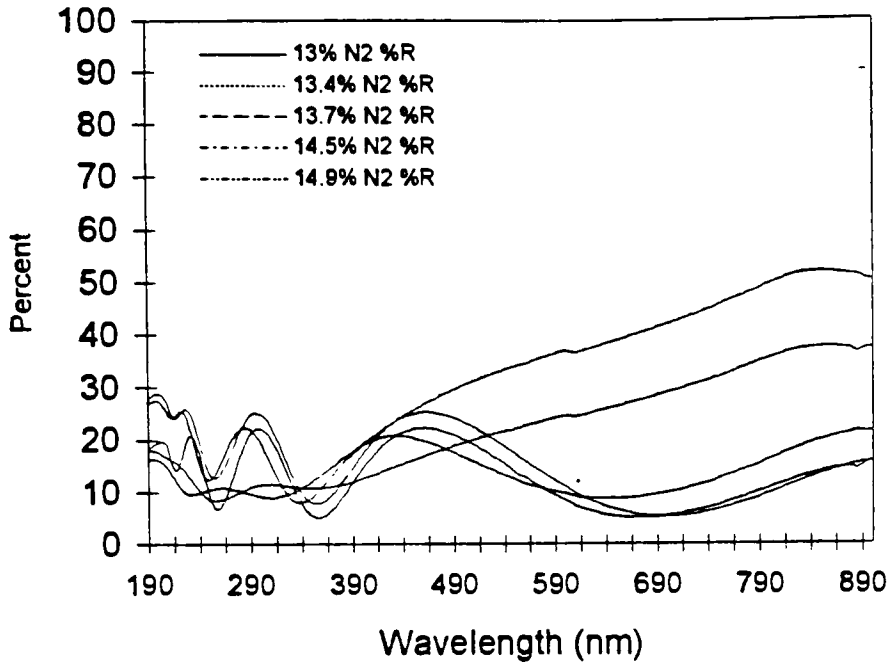

Figure 24: The reflectance spectra of a series of under-stochiometric AlN films.

From the reflectance and the transmission spectra the refractive index and the extinction coefficients were extracted. Figure 24 shows the extracted refractive index of the AlN series and Figure 25 is a representation of the extinction coefficient of the same films.

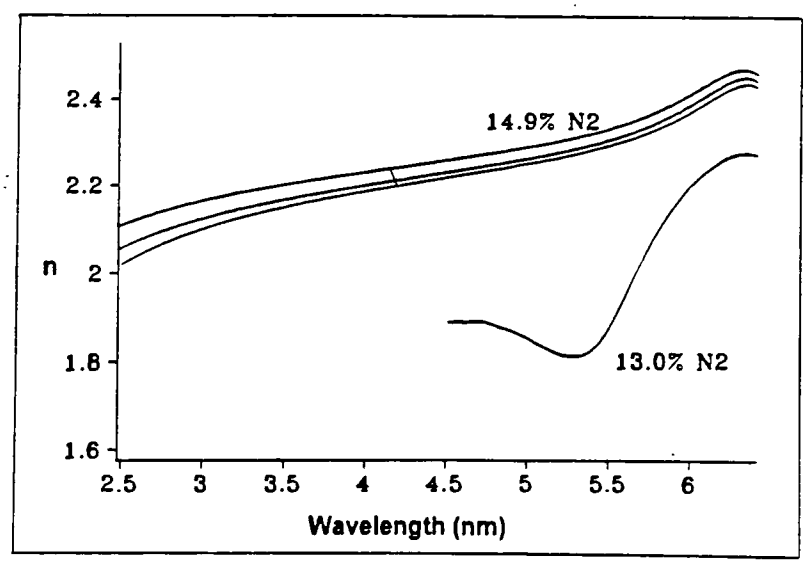

Figure 25: Refractive index values for a series of under-stochiometric AlN films.

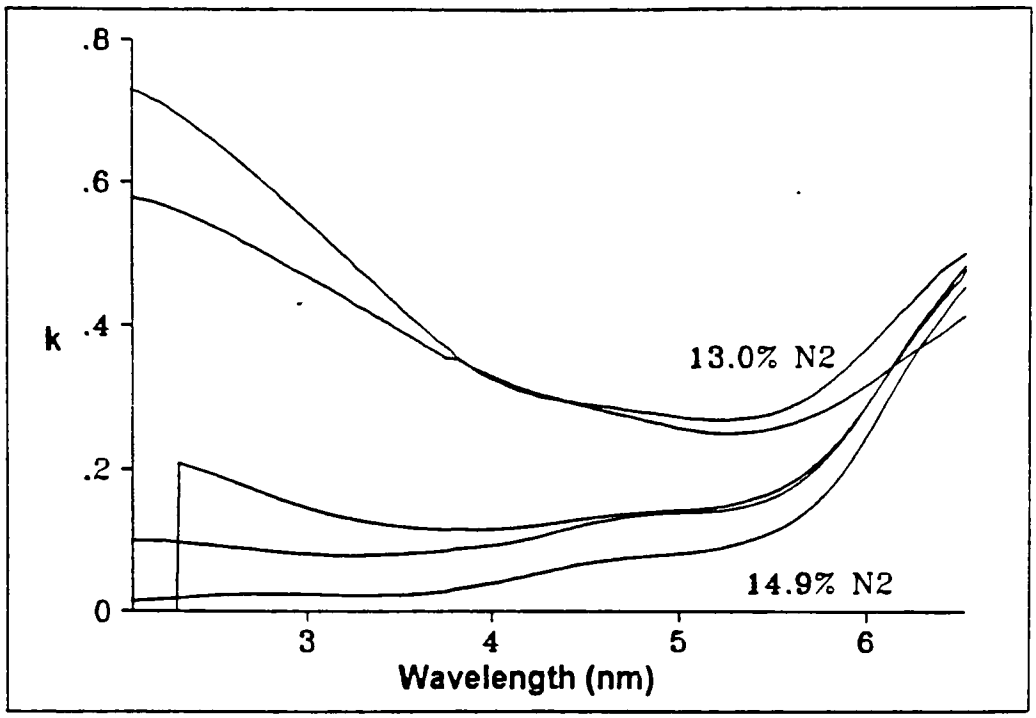

Figure 26: The extinction coefficient of the under-stochiometric AlN films.

From Figure 24 it can be seen that the extinction coefficient of the 13.0% film is actually higher in the visible regime as compared with its value at 193nm. This makes this material extremely suitable for through the mask alignment purposes. Table 8 lists the appropriate properties of these AlN films.

	13.0% N2		13.7% N2	
	193nm	500nm	193nm	500nm
n	2.26	-	2.44	
k	.404	.538	.440	.195
Thickness	765 A	765 A	670 A	670 A
Transmission	13%	36%	14.7%	72%

Table 8: Properties relevant to APSM application for the AlN films.

Hence it is possible to control the optical behavior of the AlN films. For implementing masks based on this material into production, the durability of the material after prolonged exposure to 193nm is a concern. The following section describes the experimental setup as well as the results obtained from the radiation stability experiments that were performed on the AlN films.

4.2.3 Etching

RIE results using Cl_2/Ar chemistry (58 sccm/5 sccm) power of 400W, 40mT pressure resulted in an etch rate of 97 A/min and selectivity of ~10:1 to SiO_2.

4.2.4 Radiation testing of Al/AlN films

Optimized films were tested using a Lumonics EX700 ArF excimer laser at 193nm. Films were subjected to energy levels corresponding to 1X, 10X and 100X of expected irradiance levels for mask application. This corresponds to 8 mW/cm^2, 80 mW/cm^2, and 800 mW/cm^2 on the mask plane. Typical irradiance level at the wafer plane is expected to 200mW/cm^2 for a 5X reduction exposure system. Laser repetition rate is in the 150 200 Hz range. Testing was carried on to simulate 10,000 8" wafers, assuming a resist sensitivity of about 20mJ/cm^2. Due to the excimer radiation exposure either the film thickness changes because of the impact of high energy photons, or there could be a change in the material properties. The change in transmission was used as a metric to indicate change in the film. These measurements were performed after every 25,000 pulses up to 100,000 pulses. The actual cause for the change in transmission was not determined. Figure 26 illustrates the effect of prolonged excimer radiation exposure.

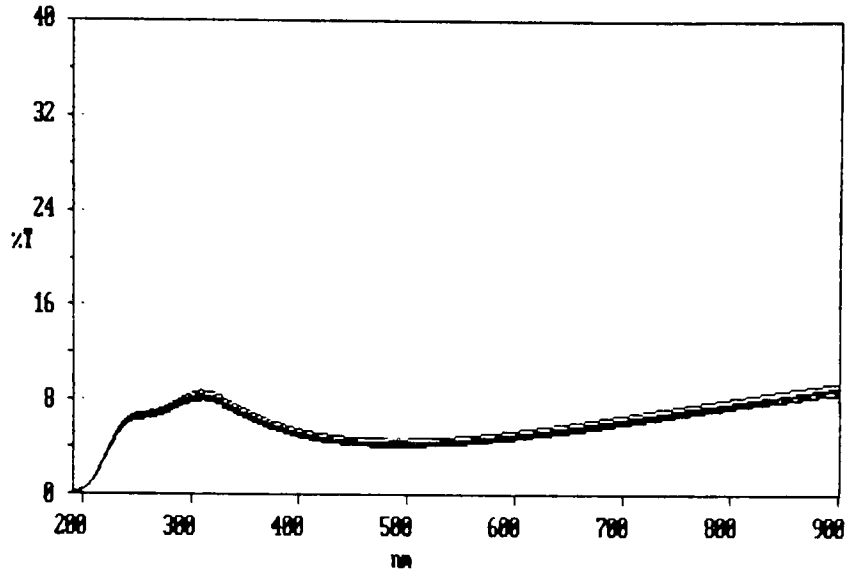

Figure 27: Transmission measurement, films become more transparent with increased exposure.

4.3 Under-stochiometric Silicon Nitride

4.3.1 Deposition and Optical Characterization

By varying the nitrogen partial pressure during reactive sputtering of silicon nitride a series of Si_xN_y films were produced. They ranged from amorphous silicon and amorphous silicon nitride. The conditions for four of these films are listed in Table 9.

Film	Power (W)	Ar flow (sccm)	N2 flow (sccm)	Time (min)	Thickness (A)
SIN423b	500W	10.4	3	45	9680
SIN423	500W	10.4	5	25	2750
SIN412	500W	10.4	15	30	2400
SIN420	500W	10.4	20	30	2620

Table 9: Deposition conditions for silicon nitride films.

Refractive index and extinction coefficient values for films deposited with 3 to 15 sccm of nitrogen flow are shown in Figure 27. These values were extracted from reflectance and transmission measurements.

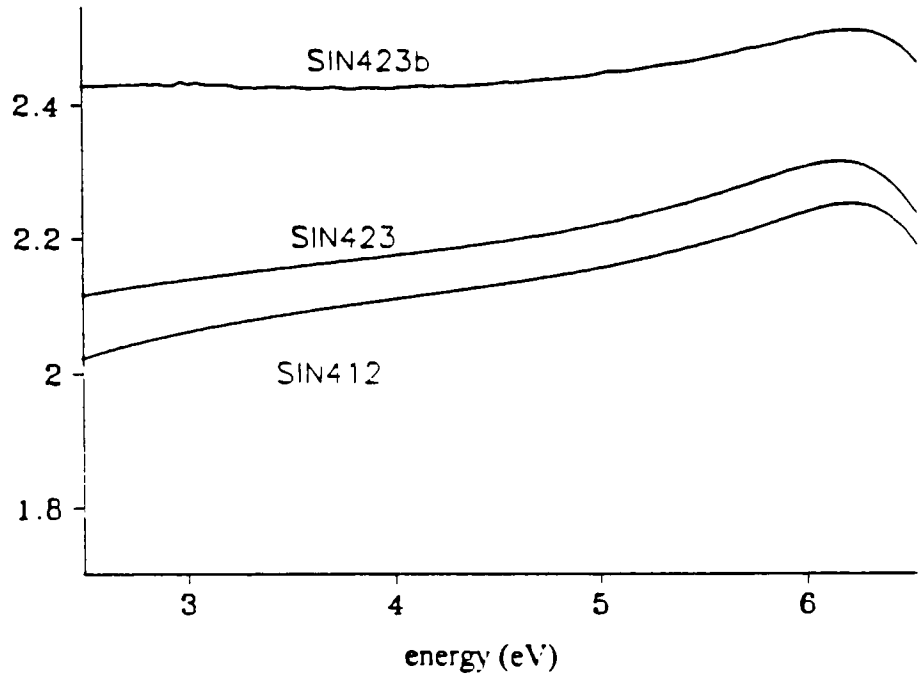

Figure 27a: Refractive index versus energy for under-stochiometric silicon nitride films.

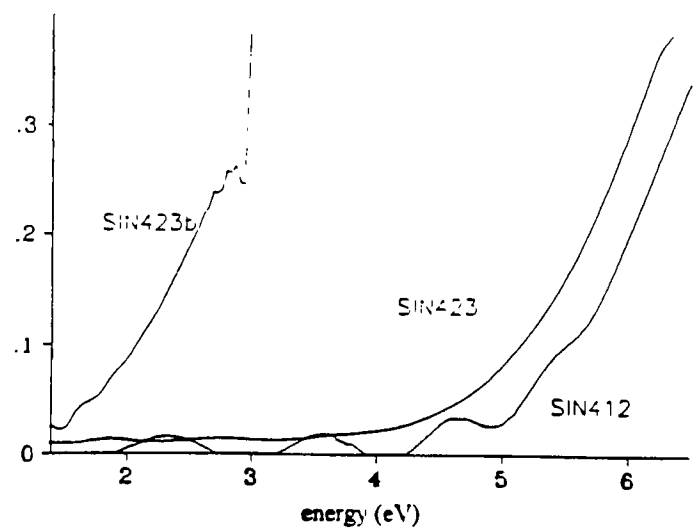

Figure 27b: Extinction coefficient versus energy for under-stochiometric silicon nitride films.

For each of these materials, n is close to that for Si_3N_4 but takes on the characteristics of Si with decreasing nitrogen. Extinction coefficient of the materials is shown in Figure 27b, where it can be seen that decreasing nitrogen levels result in an increase in the absorption at short wavelengths. Optical properties of these materials are listed in Table 10, which includes refractive index and extinction coefficient at 193nm and 500nm for these films as for stochiometric silicon and silicon nitride.

Film	n(193nm)	k(193nm)	n(500nm)	k(500nm)
Silicon	0.951	2.07	4.47	1.12
SIN423b	2.51	>0.6	2.43	0.191
SIN423	2.32	0.37	2.12	0.0028
SIN412	2.29	0.312	2.05	~0.00
SI3N4	2.68	.273	2.041	~0.00

Table 10: Optical properties of silicon nitride based materials

For a stochiometric silicon nitride film as a APSM material at 193nm the transmission is near 20% for 574 A producing a 180^0 phase shift with 21% reflectance. By introducing additional silicon, the k can be raised for improved APSM performance. Such as film SIN412 where a 780 A thick film leads to a 13% transmission with a 180^0 phase shift and 15% reflectance.

4.3.2 Etching

Plasma etching of silicon nitride can be carried out in a variety of fluorine based chemistries. Etching of silicon nitride is commonly performed in IC processing where a selectivity to SiO_2 can be as high as 10:1 using NF_3 based chemistry. At RIT using CF_4 based chemistry, an etch rate of 4100 A/min and selectivity of ~6:1 was accomplished.

4.4 Zirconium Nitride/Silicon Nitride multi-layer

4.4.1 Deposition of Zirconium Nitride

Seven series of ZrN films were deposited, varying nitrogen partial pressure, power and deposition. The deposition conditions are summarized in Table 11

Series No.	Sample Thick No.	Power (W)	N2 flow (sccm)	Ar flow (sccm)	Time (min)	(A)
I	126a	250	10	20	20	330
	126b	250	5	20	20	590
	126c	250	2	20	20	550
II	126d	250	12	20	40	1130
	126e	250	14	20	40	
	126f	250	16	20	40	
	126g	250	18	20	40	
III	214a	500	20	20	20	
	214b	500	25	20	20	
	214c	500	30	20	20	
	214d	500	35	20	20	
IV	215c	700	2.4	20	15	
	215d	700	5	20	15	
V	218a	900	5	20	10	
	218b	900	2.4	20	10	
	218c	900	10	20	10	
	218d	900	15	20	10	

VI	222a	1100	5	20	6	
	222b	1100	2.4	20	6	
VII	222c	1300	5	20	3	
	222d	1300	2.4	20	3	
VIII	318a	1100	3.5	20	1	150
	316a	1100	2.4	20	1	120
	316b	1100	1.7	20	1	260
	316c	1100	1.3	20	1	220
IX	322a	1100	2.4	20	20(rot)	460
	327a	1100	2.4	20	4	740
	327c	1100	1.1	20	4	800

Table 11: ZrN series, reactively sputtered films.

Full reflectance spectra for these films are shown in figure 28 a-d. Figure 29 is a published reflectance spectrum for zirconium nitride. Comparing the reflectance spectra for films deposited at RIT to the published result it is quite obvious that the films deposited at higher power and lower N_2 flow have spectra similar to the published results. It is believed that due to a slow sputter rate the film had a tendency to oxidize. Additionally for this work no substrate heater was used, it is believed that this leads to reduced nitrogen reactivity, other investigators have reported better quality films when they used substrate heating.

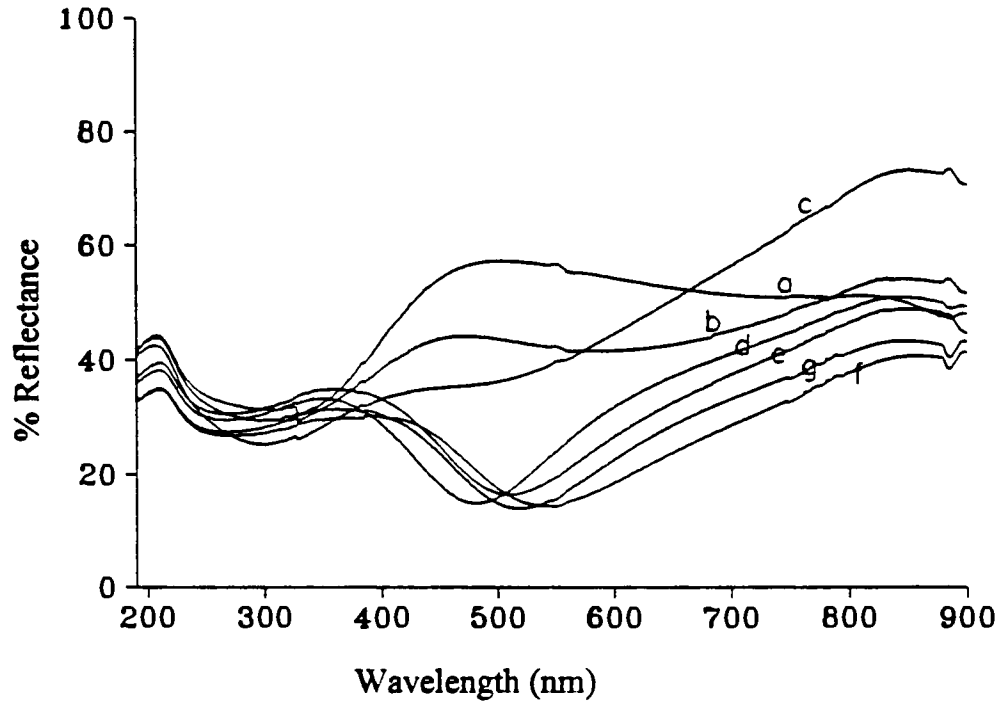

Figure 28a: Reflectance spectra of a ZrN series deposited at 500W. Film a corresponds to 10 sccm of N2 at 20 min., b is 5 sccmat 20 min., c is 2 sccm at 20 min., d is 12 sccm at 40 min., e is 14sccm at 40 min., f is 16sccm at 40 min and g is 18 sccm at 40 min.

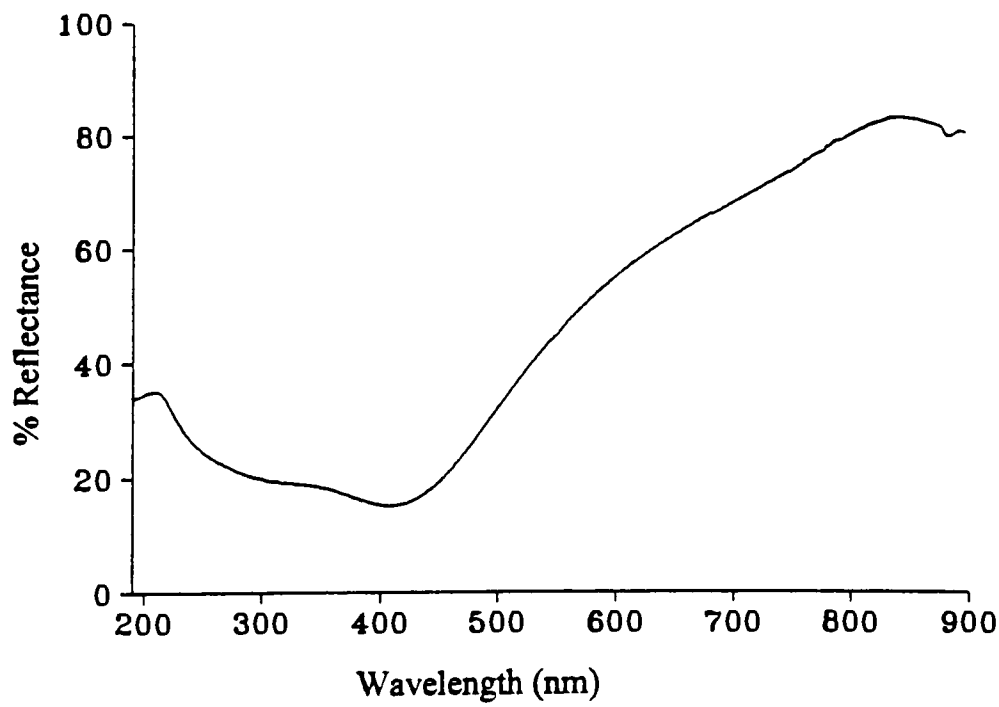

Figure 28b: Reflectance spectra for ZrN series deposited at 700W and 2.4 sccm of N2.

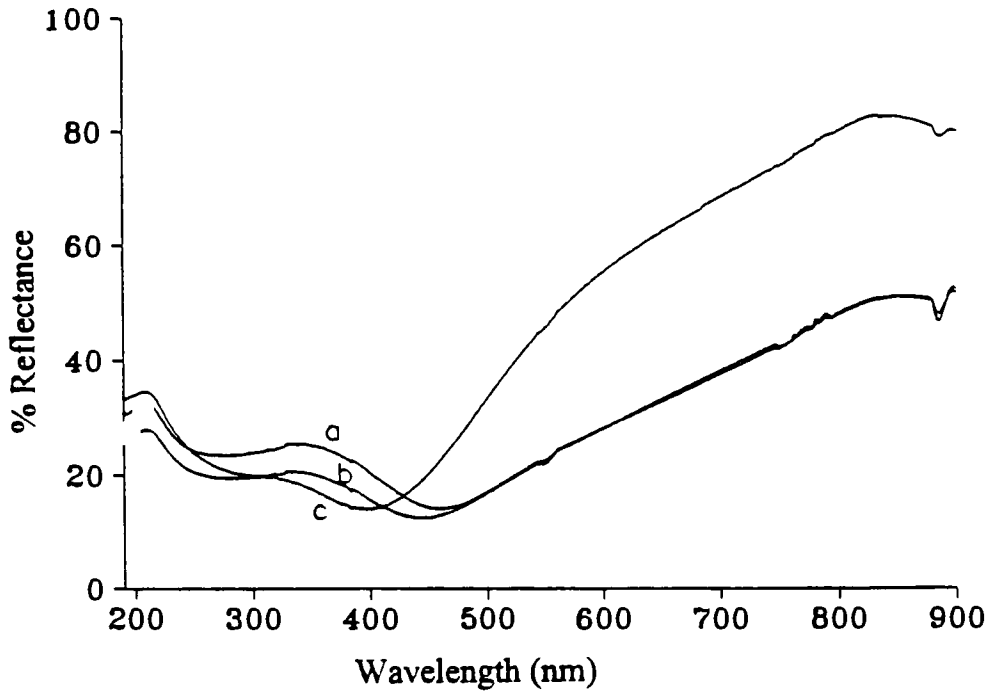

Figure 28c: Reflectance spectra for ZrN series films deposited at 900W, 15 (a), 10 (b), 2.4 (c) sccm of N2.

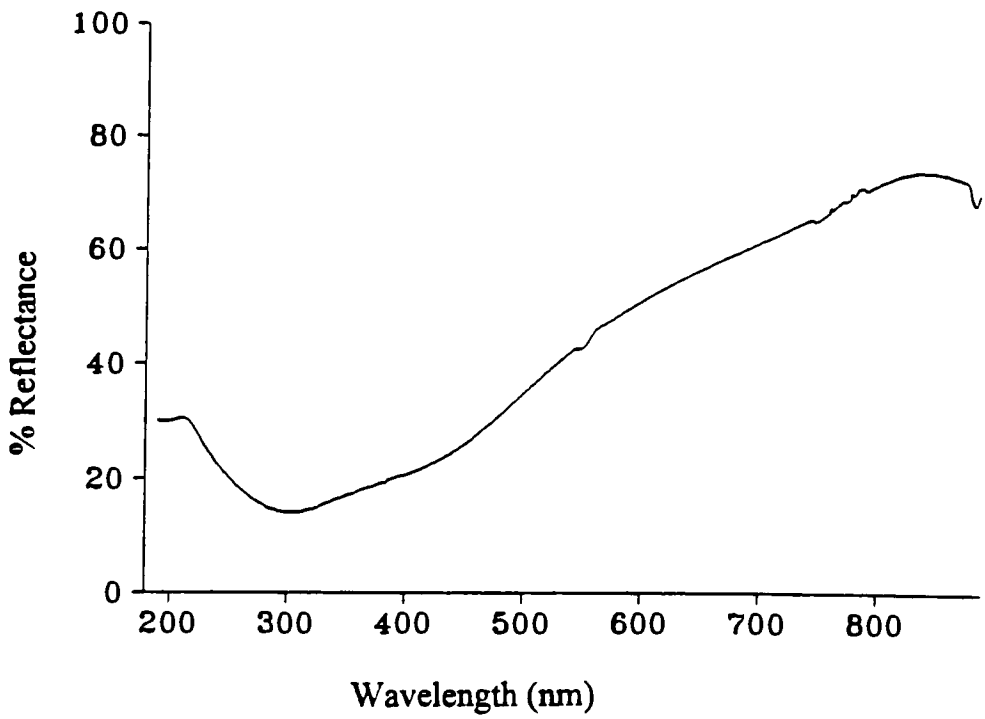

Figure 28d: Reflectance spectra for ZrN series deposited at 1100W, 1.1 sccm N_2.

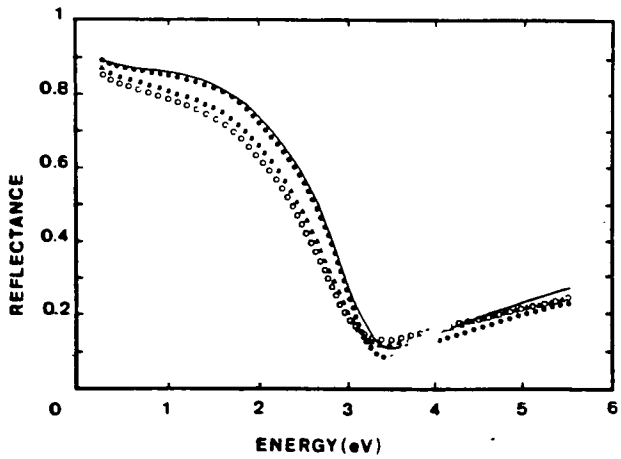

Figure 29: Published results for the reflection spectra of ZrN films.

From the transmission and reflectance data of the 1100W ZrN series, optical parameters were extracted. Figure 29a show the transmission and reflectance spectra of one of the 1100W film. Figure 29b and Figure 29c are the extracted refractive index and extinction coefficient values.

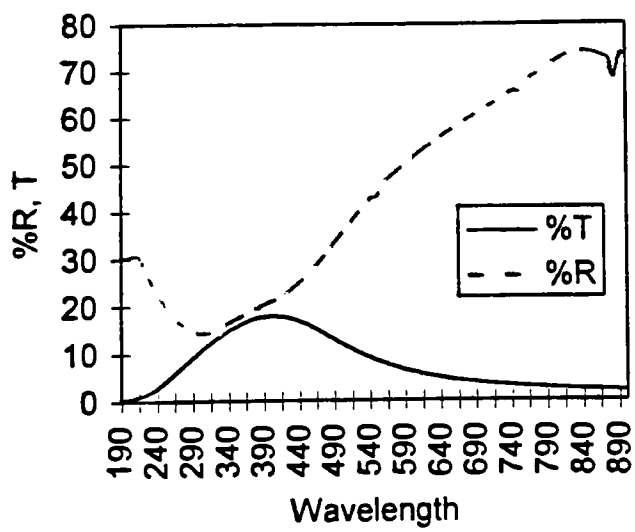

Figure 29a: Reflectance and transmission spectra of a ZrN film (327c), 800A.

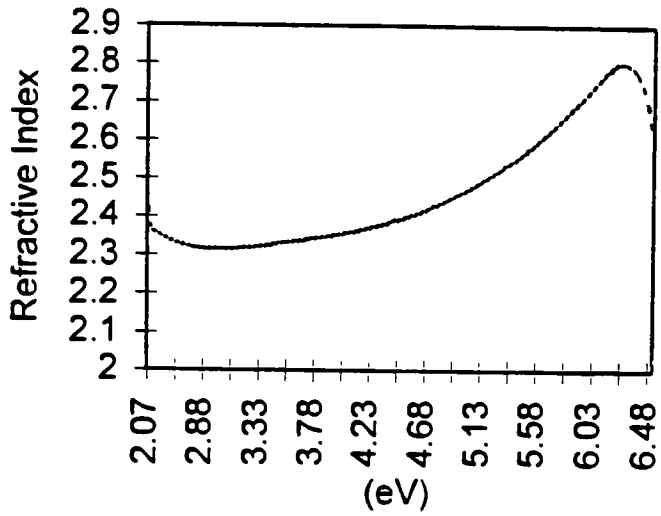

Figure 29b: Refractive index values for ZrN film 327c.

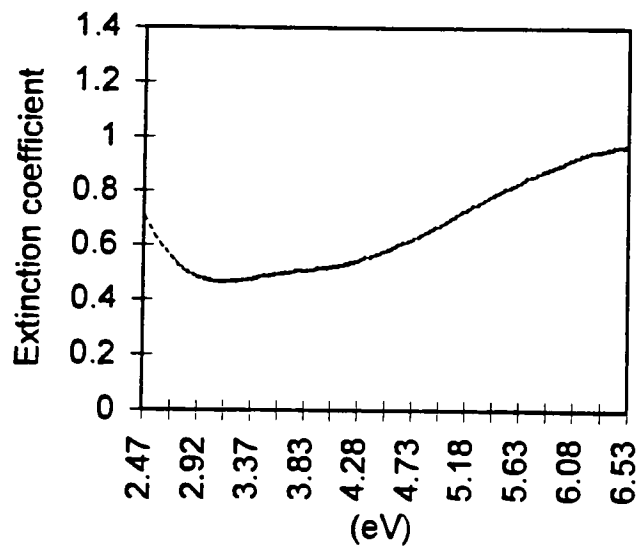

Figure 29c: Extinction coefficient data for ZrN film 327c.

Figure 30 shows the reflectance and transmission spectra of a ZrN film that was deposited using a rotating substrate stage that results in lower deposition rate.

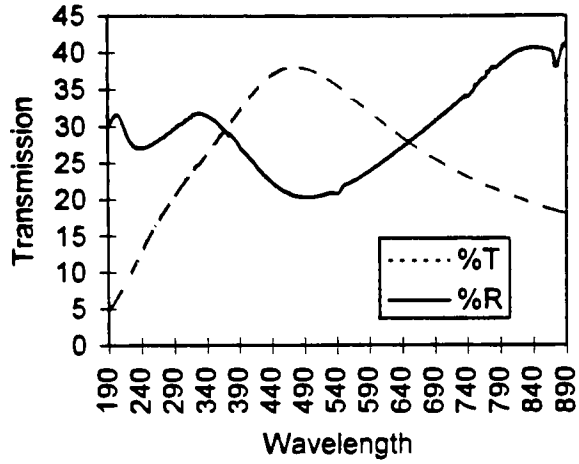

Figure 30: Reflectance and transmission spectra for ZrN film 322a, 460A

The reflectance spectrum of this film is quite different from the published results. This could be attributed to the slower deposition rate. The refractive index and extinction coefficient data in Table 12 are for the optimum ZrN film, along with the projected APSM performance.

Film	n	k	Thickness	%T (193nm)	%T (500nm)
327c	2.74	0.96	554	3.1	39

Table 12: Optical properties of ZrN film at 193 and 500nm, thickness and transmission for π phase shifting film.

It is quite obvious from the above listed values that a film similar to the type 327c would be unsuitable for phase shift application, because of its low transmission at 193nm. Zirconium Oxide films were also deposited. The Figure 31 is the reflectance and transmission spectra of a pure zirconium oxide film.

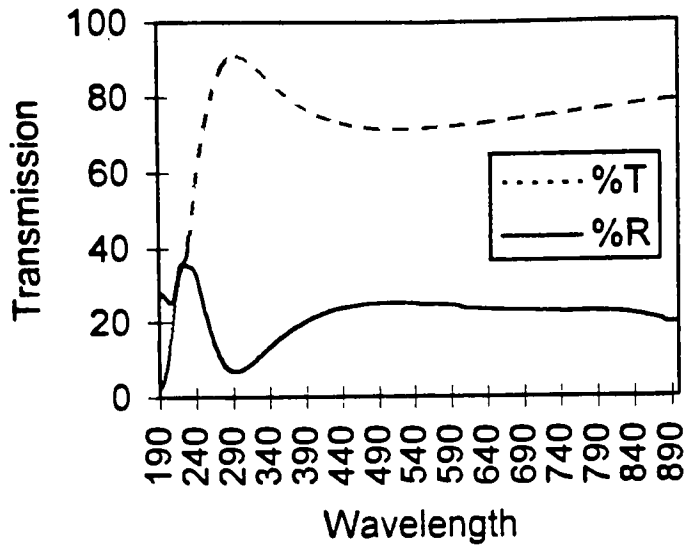

Figure 31: Reflectance and transmission spectra of a ZrO film, 645 A.

The refractive index and extinction coefficient values of ZrO were extracted. They are plotted in Figure 32a and 32b respectively.

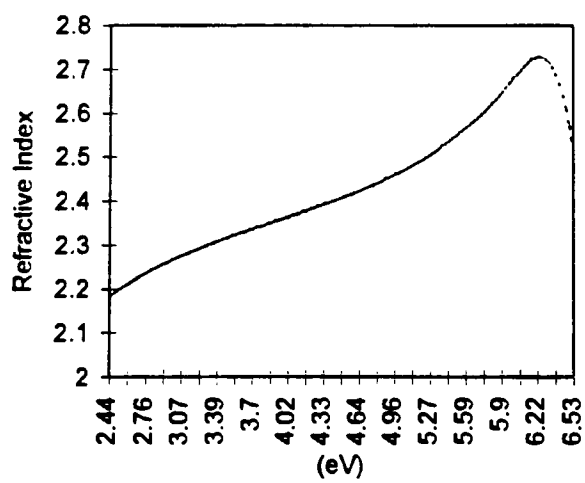

Figure 32a: Refractive index values for ZrO film.

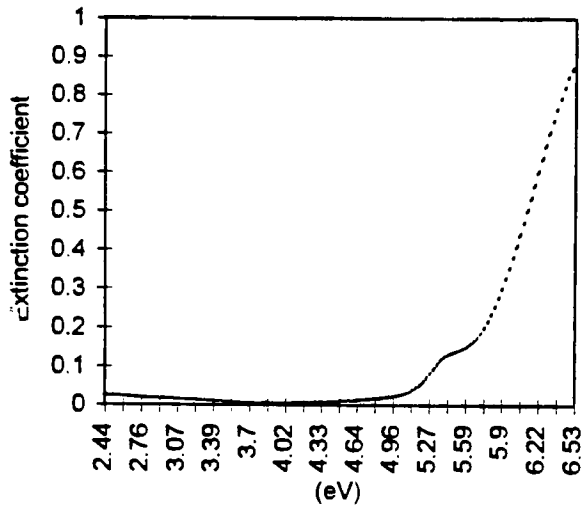

Figure 32b: Extinction coefficient values for ZrO film.

ZrO itself is unsuitable for APSM applications because of the difference in the extinction coefficient values in the visible and the UV range.

4.4.2 Radiation Stability Studies

Radiation stability studies were performed on the ZrN films in a fashion similar to that described in the AlN section. It was observed that contrary to the published data the zirconium nitride films were extremely unstable and oxidized easily. These changes are unacceptable and make the material unsuitable for manufacturing application. The change was not quantified except for transmission measurement. The material became more transparent with increased exposure. Figure 33 illustrates this fact.

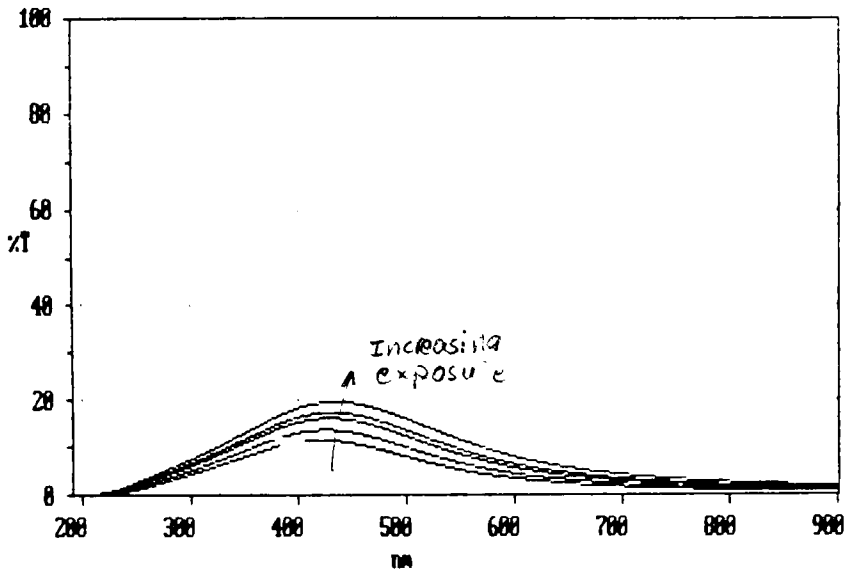

Figure 33: Increased transmission with exposure.

Hence ZrN based materials would be unsuitable for APSM applications. Therefore Zr was used in multilayer scheme with Si_3N_4. .Materials were reactively sputtered in nitrogen and argon, the silicon target was sputtered at 500W and the zirconium target was sputtered at 1500W. Table 13 summarizes the deposition parameters for two films.

Film	Power Si/Zr (W)	Ar flow (sccm)	N_2 flow (sccm)	Layers (# of)	Si:Zr time ratio	Thickness (A)
ZSN421a	500/1500	15	20	8	51:1	640
ZSN421b	500/1500	15	20	8	18:1	850

Table 13: Deposition parameters of zirconium/silicon nitride materials.

Reflectance and transmission spectra are plotted in figures 34a and 34b. As can be seen from the transmission plots that by increasing the Zr content the transmission in the visible regime can be greatly reduced, which is expected. Refractive index and extinction

coefficient plots are shown in figure 35a and 35b. It is quite obvious that material ZSN421a has the characteristic spectra of silicon nitride. Material ZSN421b has higher absorption and the extinction coefficient remains somewhat flat through the spectra. Table 14 shows optical properties of these films at 193nm and 500nm. If material ZSN421a were to be used as an APSM, for a π-phase shifting and 15% transmitting layer at 193nm the transmission in the visible would be >70%. For material ZSN421b, a π-phase shifting and 5% transmitting layer at 193nm would be 38% transparent in the visible that is acceptable.

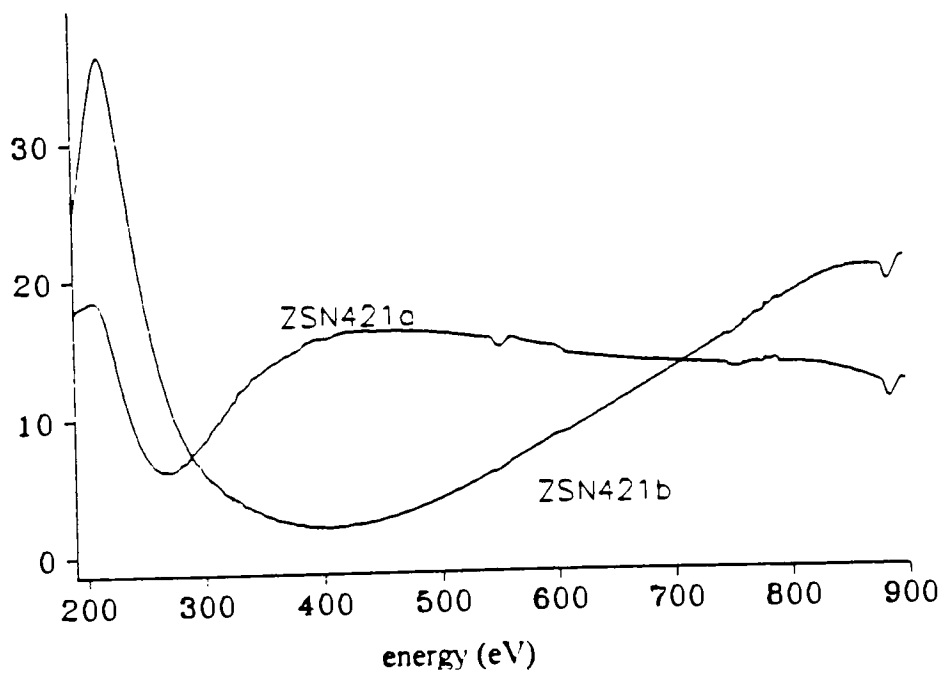

Figure 34a: Reflectance vs. wavelengths for Zr/SiN films.

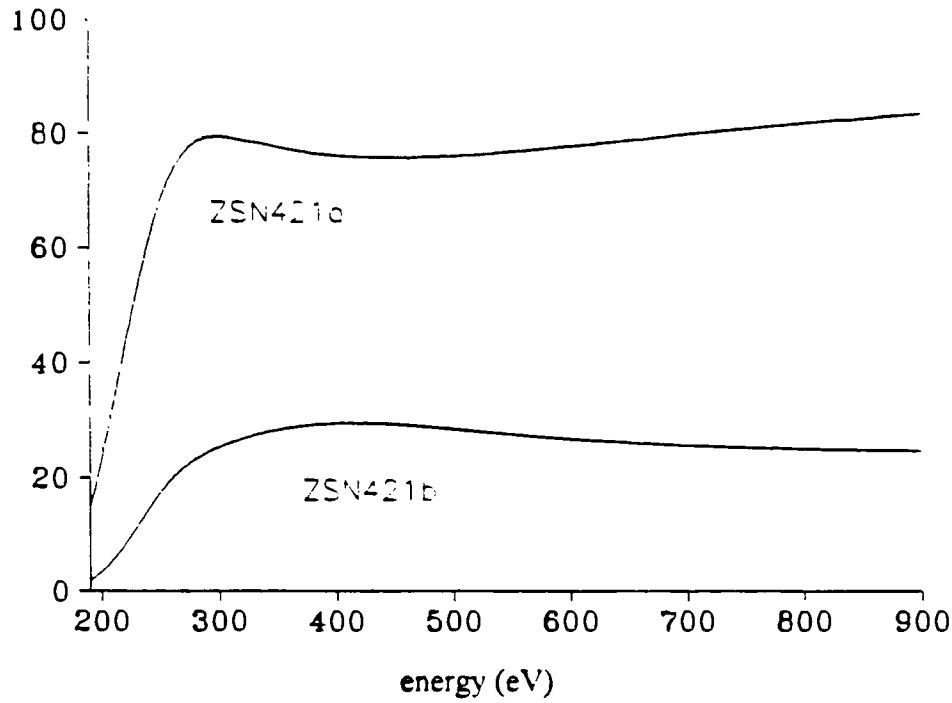

Figure 34b: Transmission vs. wavelength for Zr/SiN films.

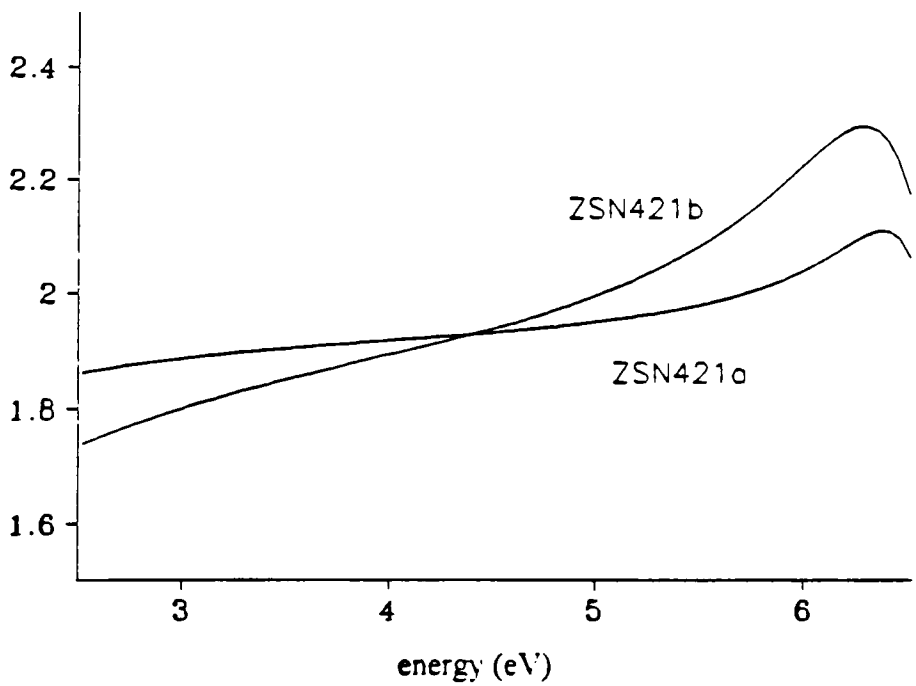

Figure 35a: Refractive index vs. energy for Zr/SiN materials

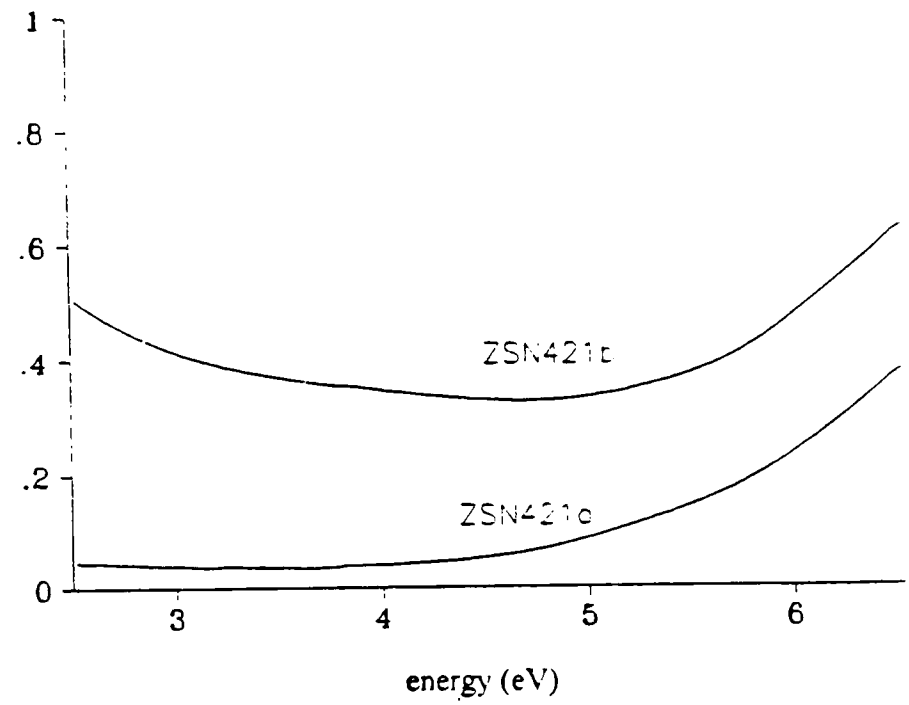

Figure 35b: Extinction coefficient versus energy for Zr/SiN materials.

Film	n(193)	k(193)	n(500)	k(500)
ZSN421a	2.11	0.354	1.86	0.047
ZSN421b	2.27	0.603	1.74	0.505

Table 14: Optical properties of zirconium-silicon nitride materials.

4.4.3 Etch studies

Some etch studies were performed on ZrN based materials before discovering the inherent instability of the material. Chlorine (58 sccm) and Argon (5sccm) based process with a power of 400W and pressure of 40 mT yield and etch rate of 47 A/min for ZrN and 79 A/min for Zr/SiN films. The etch results are summarized in Table 15.

Material	Etch rate	Selectivity	
		SiO_2	Novolac
ZrN	47A/min	4.7:1	0.02:1
Zr/SiN	79A/min	7.9:1	0.04:1

Table 15: Etch rate and selectivity of ZrN and Zr/SiN based materials.

Additionally several other multi-layer structures containing silicon nitride and a metallic component have been deposited. These materials are still being evaluated and the work would be completed at a later date. The following section would briefly describe these additional materials.

4.5 Tantalum and silicon nitride multilayer

Several films with a layered structure composed of stochiometric silicon nitride and tantalum have been deposited. The following table summarizes the deposition conditions.

	Power (W)	Ar flow (sccm)	N_2 flow (sccm)	Sputter Time (min)	Thickness (A)
Ta/SiN1	1000	15	0/15	.2/.3	640
Ta/SiN2	1000	15	0/15	.3/.3	810
Ta/SiN3	1000	15	0/15	.2/.4	930

Table 16: Sputter conditions for tantalum nitride silicon nitride multi-layer material.

Tantalum was deposited first followed by silicon nitride. This process was repeated till there were five layers of each material. The transmission spectra of these films are described in Figure 36.

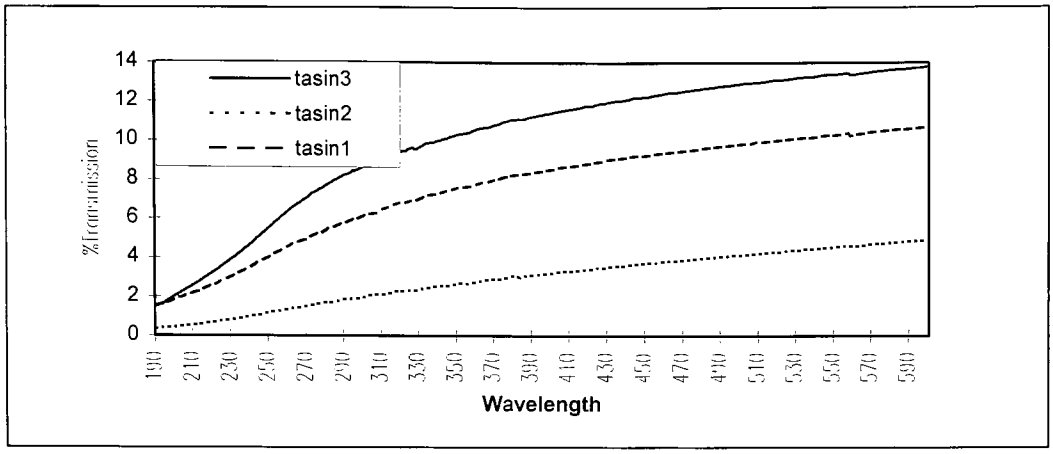

Figure 36: Transmission spectra of tantalum nitride silicon nitride series.

As can be seen from these plots, the transmission of the film decreases as the amount of tantalum is increased in the film. Also, the difference in transmission at 193 nm and 500 nm is small, which may make this suitable for APSM applications. Figure 37 is the reflectance spectra of these films.

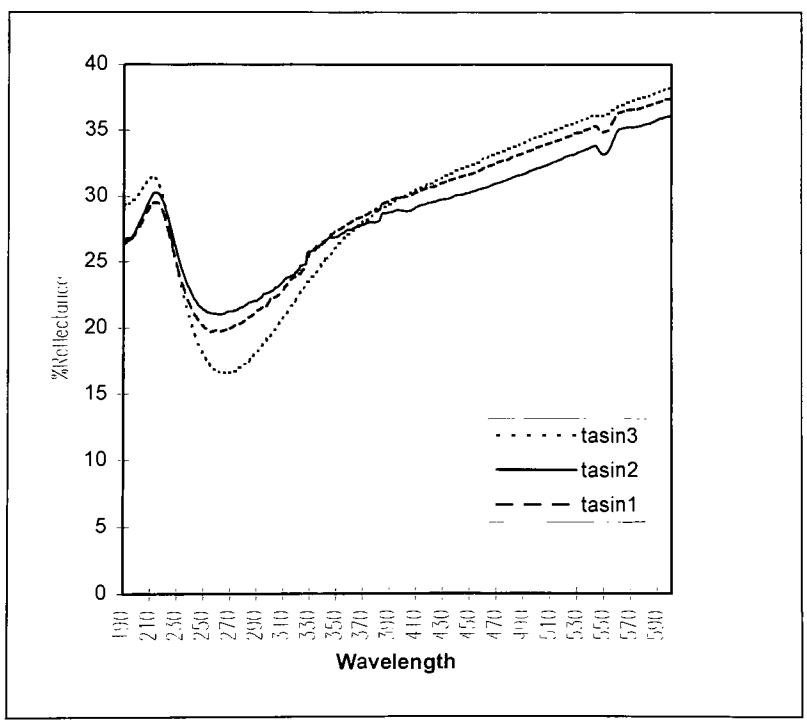

Figure 37: Reflectance spectra of tantalum nitride silicon nitride series.

Further investigation into the properties of tantalum nitride silicon nitride multi-layer is continuing since from the optical data extracted thus far this material may have the desired properties.

4.6 Tantalum nitride and silicon nitride multi-layer

A series of films composed of multi-layer of tantalum nitride and silicon nitride were also deposited. It was believed that a metallic nitride can be added to silicon nitride to darken the film and hence make it useable as a phase shift material. The following table summarizes the deposition conditions for this material.

	Power (W)	Ar flow (sccm)	N_2 flow (sccm)	Sputter Time (min)	Thickness (A)
TaN/SiN3	1000	15	15/15	.3/.3	485
TaN/SiN4	1000	15	15/15	.1/.6	510
TaN/SiN5	1000	15	15/15	.1/.4	300
TaN/SiN6	1000	15	15/15	.2/.2	587
TaN/SiN7	1000	15	15/15	.2/.4	960

Table 17: Sputter conditions for tantalum nitride and silicon nitride multi-layer.

Tantalum nitride was deposited first followed by silicon nitride. This process was repeated till there were five layers of each material. The transmission spectra of these films are described in Figure 37.

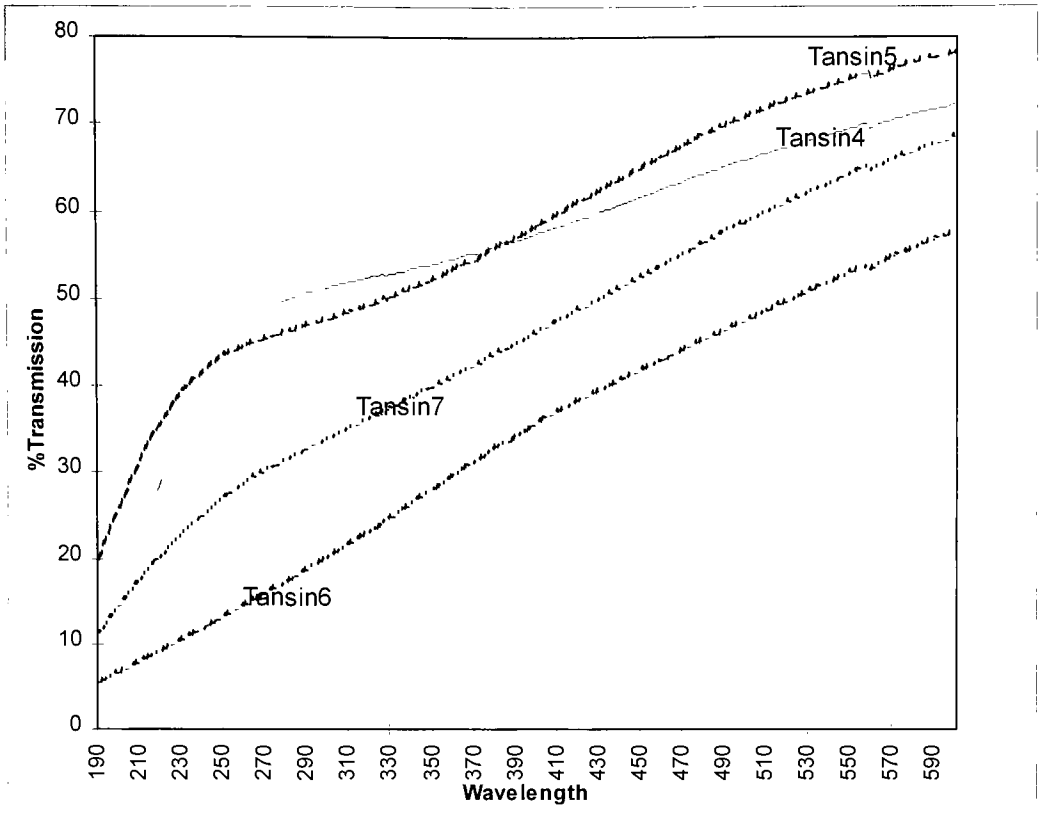

Figure 37: Transmission spectra of tantalum nitride silicon nitride series.

Once again as can be seen from these plots that the difference in transmission of these films at 193nm and 500nm is large that makes these films unsuitable for APSM application.

4.7 Zirconium nitride and silicon nitride multi-layer

Several multi-layer structures of zirconium nitride and silicon nitride were also deposited. The following table summarizes the deposition conditions.

Name	Power (W)	Ar flow (sccm)	N_2 flow (sccm)	Sputter Time (min)	Thickness (A)
102201	1000	20	5/5	1/2	1330
102202	1000	20	5/5	1.5/2	1520
102203	1000	20	5/5	2/1	1110

102204	1000	20	5/5	.5/2.5	1250
102504	1000	20	5/5	.5/1	700
110801	1000	20	5/5	.5/2	1260
110802	1000	20	5/5	.4/2	1240
110803	1000	20	5/5	.3/2	1200

Table 18: Sputter conditions for films composed of ZrN and SiN_x multi-layer.

Zirconium nitride was deposited first followed by the deposition of silicon nitride. This process was repeated till there were two layers of each material. The transmission spectrum of these films is described in Figure 38a and the reflectance spectrum is described Figure 38b.

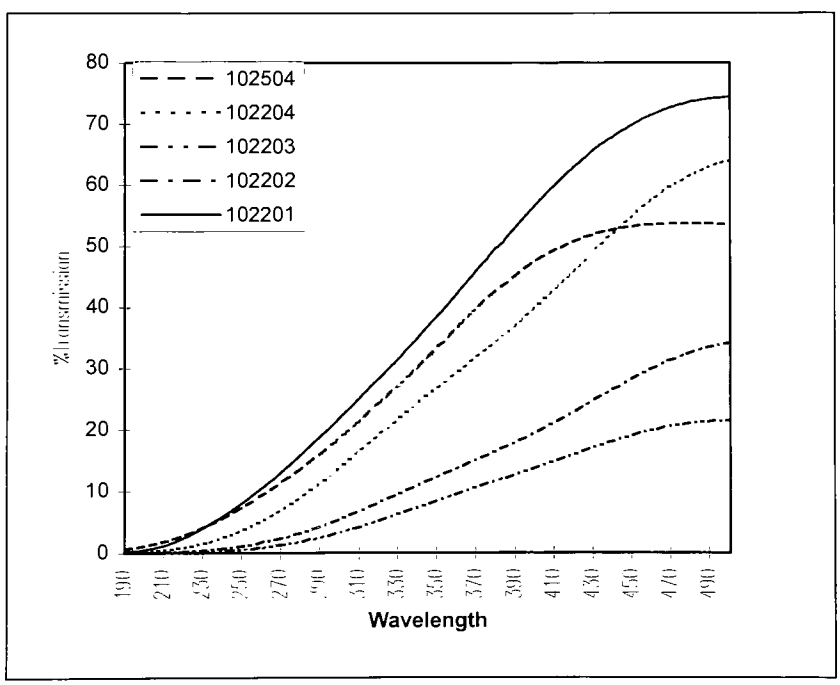

Figure 38a: Transmission spectra of zirconium nitride/ silicon nitride series.

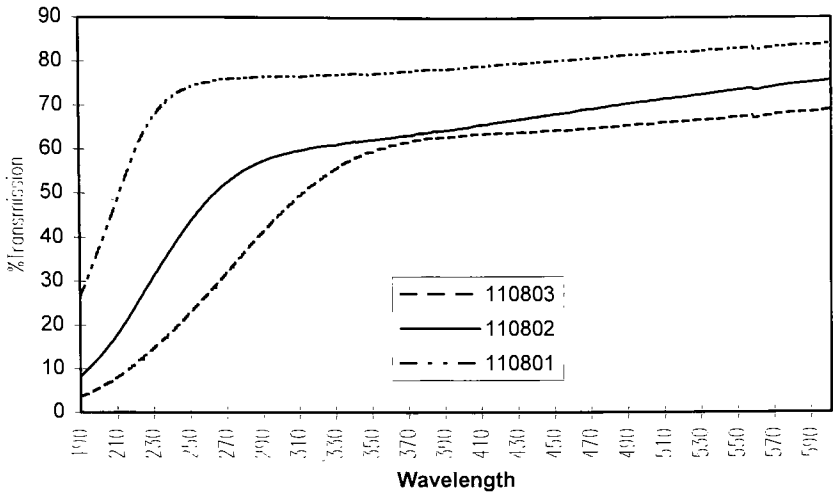

Figure 38b: Transmission spectra for ZrN/SiN multi-layer.

As can be seen from these figures the zirconium nitride silicon nitride multi-layer structure also has low transmission at 193nm and very high transmission at 500nm. This makes it difficult to engineer this material to yield properties desirable for APSM applications.

5.0 Conclusion

Several material families have been investigated as possible APSM candidates. It has been observed that by combining a variety of materials the desired optical properties can be obtained. However, the selection process is complicated by the processing and the manufacturing requirements placed on these materials. Therefore the viability of a material may be determined by properties unrelated to its optical properties at 193 nm.

Four different materials were investigated for this work. The material selection process was based on identifying materials that could be altered slightly to obtain the desired optical properties for 193 nm. Following material selection, the deposition process was adjusted to yield the desired optical properties. Finally processing and manufacturing evaluations were performed.

The first material that was investigated was molybdenum silicon oxide. The deposition process for this material could be adjusted to yield the desired optical properties at 193nm. However, this material is extremely transparent in the visible regime. Also it is believed that a large portion of this material is SiO_2 which makes it difficult to develop an etch process that has high selectivity towards fused silica. Therefore although this material meets the optical requirements for an APSM at 193 nm it fails to meet other requirements which make it unsuitable for this application.

The second material to be investigated was under-stochiometric aluminum nitride. Aluminum nitride is a dielectric or a wide band gap semiconductor, which means that the material is transparent to visible light. However, by adding a metal to aluminum nitride absorption in the visible regime can be increased. This was done by depositing aluminum rich aluminum nitride films. By adjusting the partial pressure of nitrogen the amount of aluminum in the film was controlled, which lead to very interesting optical properties. The etch behavior of this material was acceptable as well. The material was evaluated for radiation stability and it was observed that the transmission of the material increases with prolonged exposure to 193 nm radiation. It is believed that this is because of oxidation of unreacted aluminum in the film. It may be possible to circumvent this problem by layering this material such that the top layer is aluminum nitride.

Silicon nitride was the third material to be investigated. This material has been looked into for 248 nm APSM by other investigator. Also since silicon nitride is extensively used in the integrated circuit industry there is a large amount of information available on it. By adding silicon to silicon nitride the optical properties can be adjusted to meet the requirements for APSM. This was done by sputtering under-stochiometric silicon nitride. However, this material also suffers from extremely high transmission in the visible region. Recently it has been reported that under-stochiometric silicon nitride is susceptible to change when it is exposed to 248 nm radiation for a prolonged period of time. This phenomenon would most likely occur at 193 nm as well.

It was decided that the final material to be investigated would be silicon nitride layered with a metallic nitride to provide stability to the film. For this purpose zirconium nitride was selected, according to results published elsewhere it was believed that this material is extremely stable. However, the zirconium nitride films deposited at RIT were extremely susceptible to radiation damage. By using a multilayer structure of zirconium and silicon nitride it may be possible to avoid the stability problem. This material was optimized to yield the desired optical properties. The extinction coefficient of this material remains relatively flat from UV through the visible. Also this material has acceptable etch behavior. It is sufficiently selective towards fused silica. The radiation stability of this material remains to be investigated. As an afterthought several other materials were looked into as replacement for ziconium nitride in the silicon nitride zirconium nitride multilayer scheme. This work is ongoing and these materials may present the ultimate solution.

However, it is interesting to observe that the stochiometric form of the materials investigated in this work do not match the optical requirements for an APSM at 193 nm. By adjusting the deposition conditions these requirements could be met. Four different materials were investigated and all of them met the optical requirements for 193 nm APSM. The processing and manufacturing requirements were harder to meet. Aluminum nitride seems the most promising, it has suitable optical properties, the etch behavior is

acceptable and it may be possible to make the material stable to excimer radiation exposure by layering it.

6.0 References

1. Gordon Moore, "Lithography and the Future of Moore's Law." SPIE vol.2440 (1995).
2. L. F. Thompson, C.G. Wilson and M. J. Bowden, Introduction to Microlithography, American Chemical Society (1994).
3. Karen Brown, "SEMATECH and the national technology roadmap: needs and challenges", SPIE vol. 2440 (1995).
4. Burn J. Lin, "The Attenuated Phase-Shifting Mask", Solid State Technology (Jan 1992).
5. M. Born and E. Wolf, Principles of Optics, Pergamon Press (1980).
6. K. Ronse et. al, "Optimization of the optical phase shift in attenuated PSM and application to quarter micron deep-UV lithography in logics", Microelectronic Engineering, vol. 23, 133 (1994).
7. Shahid Butt, "Attenuated PSM for 193 nm lithography", Proc. of the Annual Microelectronic Engineering Conf. (1995).
8. Bruce Smith, Sulyeman Turgut, "Phase shift masks issues for 193 nm lithography", SPIE vol. 2197 (1994).
9. Rolf E. Hummel, Electronic Properties of Materials, Springer Verlag (1993).
10. J. L. Vossen, W. Kern, Thin film processes II, Academic Press (1991).
11. S. Wolf, R. Tauber, Silicon processing for the VLSI era vol. 1, Lattice Press (1986).
12. D. M. Manos, D. L. Flamm, Plasma Etching an Introduction, Academic Press (1989).
13. CRC Handbook of Chemistry and Physics, CRC Press (1996).